Supporting Information

Hacking a Brønsted Photoacid to Capture and Directly Release a Lewis Acid: Applied to CO_2 Photorelease

Berk Delibas[1], Sumit Sahu[1], Dani Cotton[1], Hayden Harkins[2], Andrew Petit[2], Joaquín Rodríguez-López[3], and Jahan M. Dawlaty*[,1]

[1]Department of Chemistry, University of Southern California, Los Angeles, California 90089, United States

[2]Department of Chemistry and Biochemistry, California State University-Fullerton, Fullerton, California 92834, United States

[3]Department of Chemistry, University of Illinois Urbana−Champaign, Urbana, Illinois 61801, United States; Beckman Institute for Advanced Science and Technology, University of Illinois Urbana−Champaign, Urbana, Illinois 61801, United States

E-mail: dawlaty@usc.edu

Table of contents

Section S1. Methods

Chemicals

2-naphthol (Sigma-Aldrich, ≥98%), 6-bromo-2-naphthol (Sigma-Aldrich, 97%), 6-cyano-2-naphthol (Sigma-Aldrich, 97%), 6-methoxy-2-naphthol (Sigma-Aldrich, ≥97%), Sodium Hydride (NaH, Sigma-Aldrich, 60 % dispersion in mineral oil), Triethylamine (TEA, Sigma-Aldrich, ≥99.5%, liquid), Tetrahydrofuran (THF, Sigma-Aldrich), Acetone (Fisher Scientific Company), Methanol (Sigma-Aldrich), HPLC grade water (Sigma-Aldrich), Hexane (Sigma-Aldrich, ≥99%) were commercially acquired and used as received without any further purification. Solvents used in sample preparation was dried under activated 3Å molecular sieves overnight to drive away water. CO_2 with 99.99% purity was supplied from a compressed gas canister.

Synthesis

All solvents used in sample preparation were thoroughly dried over activated 3 Å molecular sieves overnight to ensure the removal of residual moisture. A 10 mL solution of 2-naphthols (0.25 M) in uninhibited anhydrous THF was transferred into a nitrogen-purged round-bottom flask containing sodium hydride. The reaction mixture was stirred continuously under an inert atmosphere overnight to facilitate complete deprotonation. Following this, the mixture was filtered to remove any unreacted solids, and the resulting sodium naphtholate solution was used directly for subsequent experiments. To generate the naphthylcarbonate species, the filtered sodium naphtholate solution was exposed to a CO_2 atmosphere (1 atm) by maintaining a CO_2 headspace in the sealed reaction vessel. The solution was stirred briefly (~1 minute) to ensure adequate equilibration. Aliquots of this CO_2-treated solution were used for further characterization. For photo-release experiments, the CO_2-loaded solution was transferred into a well-sealed FTIR cell. The cell was then irradiated with 340 nm THORLABS M340L5 LED at half power to induce the release of CO_2 from the naphthylcarbonate species.

Instrumentation

All the vibrational spectra were recorded using a Nicolet iS50 FTIR spectrometer under a dry air purge. All the samples (0.25M) were sandwiched between two CaF_2 windows with a ~15μm spacer to clearly observe the peak shape and position without saturating the DTGS detector.

The spectra were measured with a resolution of 1 cm^{-1}. The same cell was used for collecting UV-Vis absorption spectra. FTIR cell was sealed with epoxy resin to make it air tight. Exact path length (~34μm) of the cell was determined by the fringe pattern obtained when IR spectrum was recorded with air in between two CaF_2 windows. All the NMR spectra were collected in Varian 400MR MHz Spectrometer using 0.25M samples dissolved in pure THF. Spectra were calibrated using THF peak and were processed using MestreNova 14.3.0 software. Fluorescence spectra were collected using Horiba NanoLog spectrofluorometer using 0.25M samples in 1cm quartz cuvettes. Slit width were optimized to not saturate the detector due to highly concentrated samples used.

Computation:

Ground state and excited state geometry optimizations and vibrational frequency calculations were performed using density functional theory (DFT) at the ωB97X-D/def2-SVPD level of theory.[2,3] The Restricted Open-Shell Kohn Sham (ROKS) methodology was used to achieve state-specific excited state geometry optimizations and frequency calculations.[4–6] All stationary points were verified to have the appropriate number of imaginary frequencies. All calculations employed a polarizable continuum model (PCM) parameterized for THF and were performed using Q-Chem 6.2. For the molecular anions, we also considered multiple conformations of the contact ion pair with Na^+.[7]

A number of spectroscopic observables were calculated in this study. We obtained harmonic vibrational frequencies to compare to the experimental IR spectra by re-optimizing the ground state geometries using ωB97X-D/def2-TZVPPD. The vertical absorption (emission) energy gaps were obtained by calculating the ADC(2)/def2-TZVPD excited state energies at the ground (excited) state optimized geometries.[8,9] Finally, we calculated the $S_0 \rightarrow S_1$ adiabatic energy gaps by subtracting the S_1 energy at the excited state optimized geometry with the MP2/def2-TZVPD energy at the ground state optimized geometry.

We described the thermodynamics and kinetics of CO_2 release in the ground and excited state by developing reaction coordinate diagrams at the ωB97M-V/def2-QZVPD//ωB97X-D/def2-SVPD level of theory.[10] We additionally performed a relaxed excited state potential energy scan stretching the O-C bond between the 2-naphtholate and the CO_2 using ROKS-ωB97X-D/def2-SVPD. At each optimized geometry along the scan, we evaluated the energies of the low-lying singlet and triplet excited states using ADC(2)/def2-TZVPD.

To better understand the dative bond between 2-naphtholate and CO_2, we performed energy decomposition analysis (EDA) at the ground and excited state geometries using the second-generation absolutely localized molecular orbitals (ALMO-EDA II) methodology at the ωB97X-D/def2-TZVPPD level of theory.[11] We used the state-specific maximum overlap method (MOM) to perform the EDA analysis on a non-Aufbau excited electron configuration.[12] Note that the MOM approach does not conserve spin, so these calculations have $\langle S^2 \rangle \approx 1$. We compared the ground and excited EDA analysis adiabatically.

Section S2: Characterization of various Naphthol species

Section S2.1: Spectroscopic measurements

The following are the FTIR, NMR, UV-Vis, and emission spectra of naphthol, naphtholate and naphthylcarbonate species of 2-naphthol, 6-bromo-2-naphthol, and 6-methoxy-2-naphthol respectively. Data was collected as explained in the methods. FTIR data presented here have been subjected to solvent (THF) subtraction to make it more readable.

6-bromo-2-naphthylcarbonate has low solubility in THF and therefore its spectrum has very small amounts of carbonate signal as formed carbonate crashes out of the solution. Unfortunately, due to its low concentration, we could not do a Förster cycle analysis on 6-bromo-2-naphthylcarbonate.

The NMR data was collected from highly concentrated samples as we wanted to make sure we could keep our characterizations constant between all the methods above. We believe this highly concentrated sample generated dimer-like structures which are evidenced by the splitting of almost all NMR peaks into two. We have reported them as if they are one peak in our analysis as the dimer structure likely does not make any difference to our work.

For brevity 2-naphthol, 2-naphtholate, 2-naphthylcarbonate, 6-methoxy-2-naphthol, 6-methoxy-2-naphtholate, 6-methoxy-2-naphthylcarbonate, 6-bromo-2-naphthol, 6-bromo-2-naphtholate, 6-bromo-2-naphthylcarbonate will be referred as 2-NpOH, 2-NpO^-, 2-$NpOCOO^-$, 6-MeO-2-NpOH, 6-MeO-2-NpO^-, 6-MeO-2-$NpOCOO^-$, 6-Br-2-NpOH, 6-Br-2-NpO^-, 6-Br-2-$NpOCOO^-$ respectively in this SI.

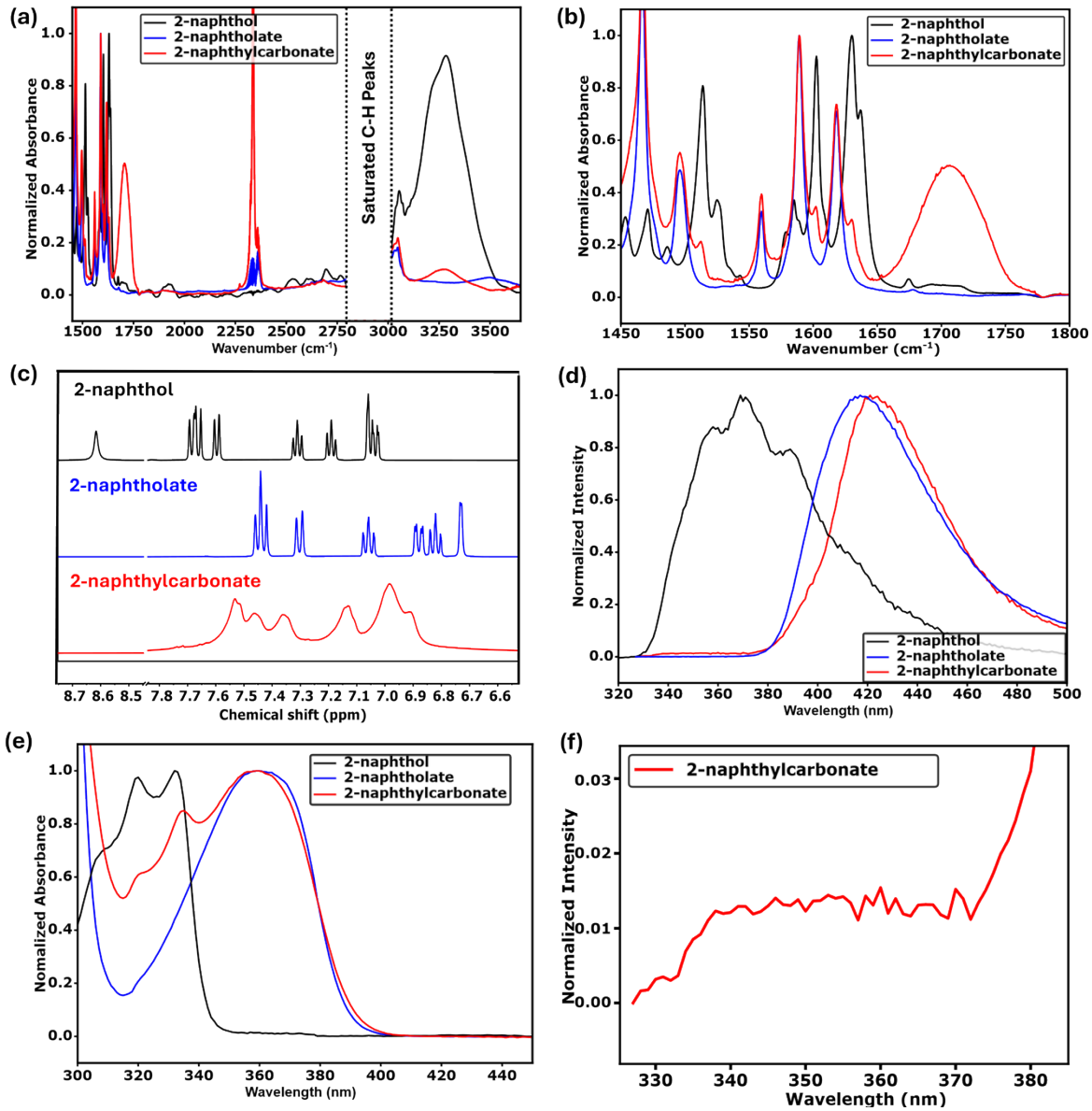

Figure S1 showing the (a) FTIR (full scale), (b) FTIR (ring modes and asymmetric carbonate frequency region), (c) NMR, (d) Absorption, (e) Emission spectra of 2-NpOH (black), 2-NpO$^-$ (blue), and 2-NpOCOO$^-$ (red), and (e) Zoomed in emission spectra of 2-NpOCOO$^-$.

For 2-NpOH: ^{1}H NMR (500 MHz, thf) δ 8.63 (s, 1H), 7.69 (d, J = 11.6, Hz, 2H), 7.61 (d, J = 8.2 Hz, 1H), 7.32 (t, J = 6.9 Hz, 1H), 7.20 (t, J = 6.8 Hz, 1H), 7.07 (s, 1H), 7.05 (d, J = 8.7 Hz, 1H).

For 2-NpO$^-$: ^{1}H NMR (400 MHz, cdcl$_3$) δ 7.45 (m, 2H), 7.31 (d, J = 8.3 Hz, 1H), 7.07 (t, J = 6.8 Hz, 1H), 6.89 (d, J = 8.8 Hz, 1H), 6.83 (t, J = 6.8 Hz, 1H), 6.74 (s 1H).

Peak assignment to the 2-NpOCOO$^-$ are not done due to the smeared nature of the spectra. Main features between 7.6 to 6.9 ppm.

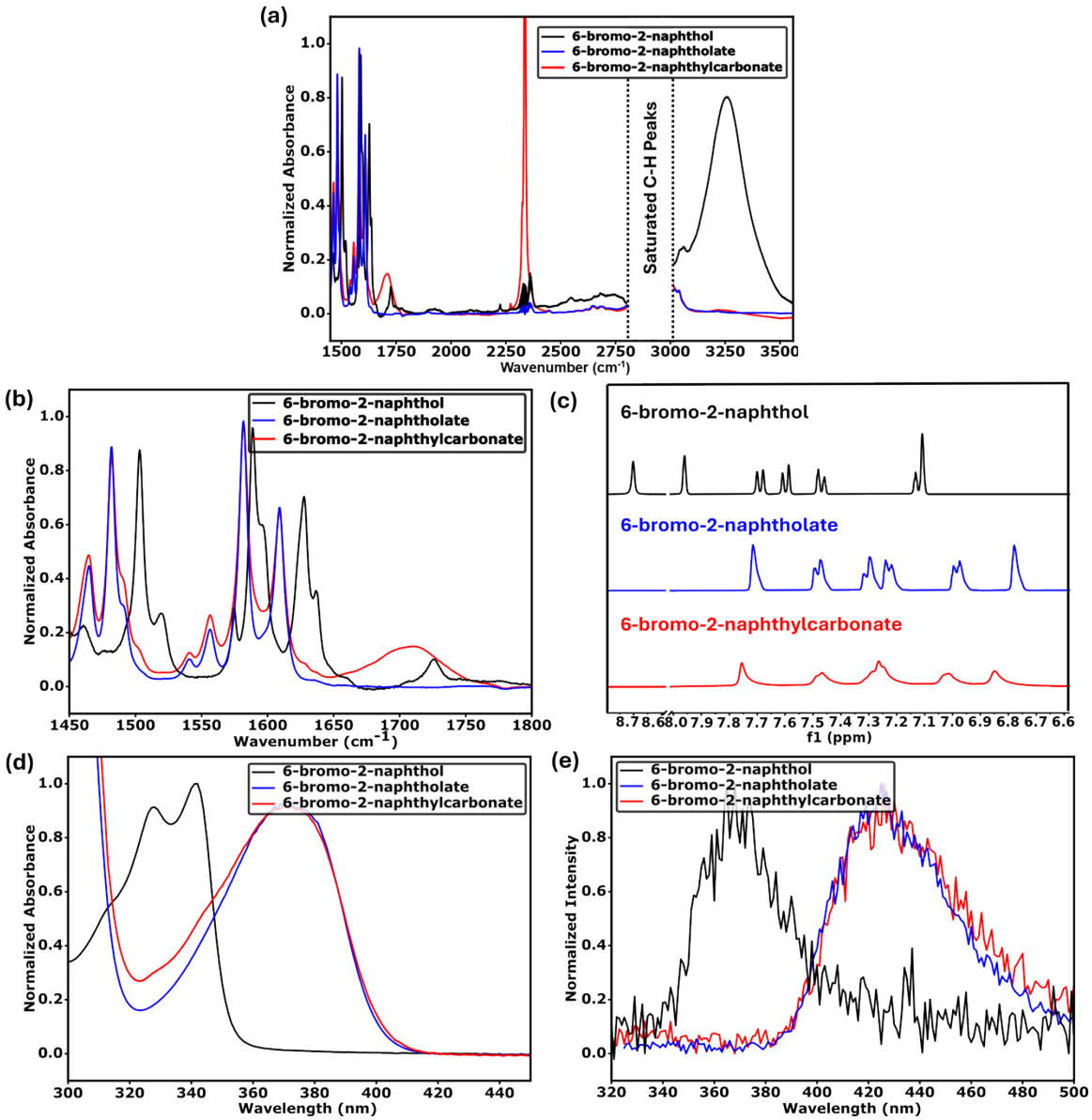

Figure S2 showing the (a) FTIR (full scale), (b) FTIR (ring modes and asymmetric carbonate frequency region), (c) NMR, (d) Absorption, and (e) Emission spectra of 6-Br-2-NpOH (black), 6-Br-2-NpO$^-$ (blue), and 6-Br-2-NpOCOO$^-$ (red)

For 6-Br-2-NpOH: ^{1}H NMR (500 MHz, thf) δ 8.63 (s, 1H), 7.69 (d, J = 11.6, Hz, 2H), 7.61 (d, J = 8.2 Hz, 1H), 7.32 (t, J = 6.9 Hz, 1H), 7.20 (t, J = 6.8 Hz, 1H), 7.07 (s, 1H), 7.05 (d, J = 8.7 Hz, 1H).

For 6-Br-2-NpO$^-$: ^{1}H NMR (400 MHz, cdcl$_3$) δ 7.70 – 7.58 (s, 1H), 7.41 (d, J = 9.0 Hz, 1H), 7.24 (d, J = 9.2 Hz, 1H), 7.16 (d, J = 9.0 Hz, 1H), 6.91 (d, J = 9.2 Hz, 1H), 6.71 (s, 1H).

Peak assignment to the 6-Br-2-NpOCOO$^-$ are not done due to the smeared nature of the spectra. The main features mostly follow that of naphtholate due to low carboate conentration for this sample.

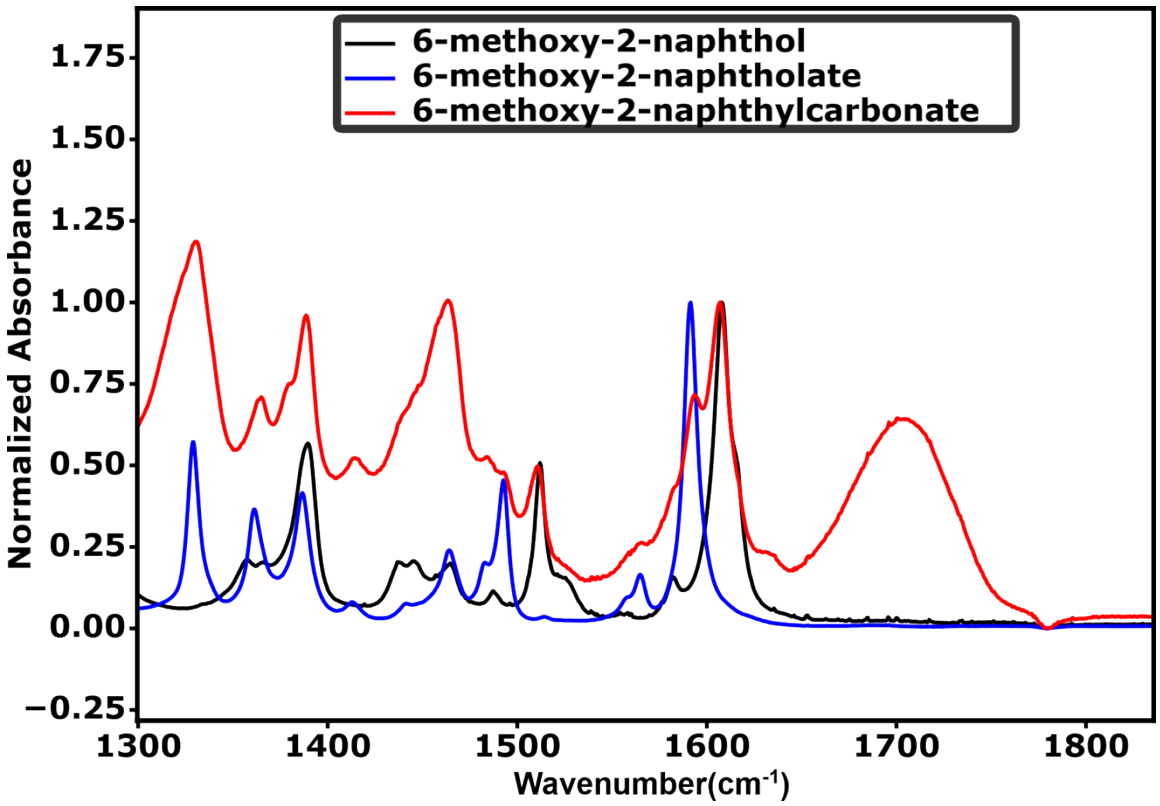

Figure S3. showing the FTIR spectrum (normalized to ring modes) showing that the ring modes of the 6-MeO-2-NpO$^-$ shift to lower frequencies and overlap with other peaks.

Experimental characterization of 6-cyano-2-naphthol is not shown in this work and is not included in the main manuscript. The naphtholate version of it is not very soluble in THF. Furthermore, 6-cyano-2-naphtholate reacts in small amounts with CO_2. Unfortunately, the small amount of formed carbonate is almost completely insoluble in THF. Since data from this sample is not possible to parse in a meaningful way, we have decided to omit it in this study. However, it was used in the computational section of this SI and further details can be found below. The inability of 6-cyano-2-naphtholate to form a CO_2 adduct, in contrast to 2-NpO$^-$, 6-Br-2-NpO$^-$, and 6-MeO-2-NpO$^-$, can be attributed to the strong electron-withdrawing nature of the cyano substituent. The –CN group reduces the electron density on the naphtholate through both inductive and resonance effects, thereby significantly diminishing its nucleophilicity and affinity towards CO_2. In contrast, the –Br group is only weakly withdrawing, which slightly decreases the nucleophilcity of 6-Br-2-NpO$^-$ towards CO_2. However, 6-MeO-2-NpO$^-$ is the most reactive toward CO_2 because the methoxy group is a strong electron donating group which enhances the nucleophilcity of 6-MeO-2-NpO$^-$ to attack CO_2 and form strong adduct. This point have been supported further computationally and can

be found in the main paper. Although quantitative analysis is not possible from the data we present, qualitatively it is possible to observe the methoxy substituted naphthol forming the most carbonate while the bromine substituted naphthol forms the least by comparing the relative peak sizes of naphtholate versus carbonate in figure S4. Methoxy substituted sample has almost negligible amounts of naphtholate present after reacting with 1 atm of CO_2 while bromine substituted sample is almost completely in its naphtholate form.

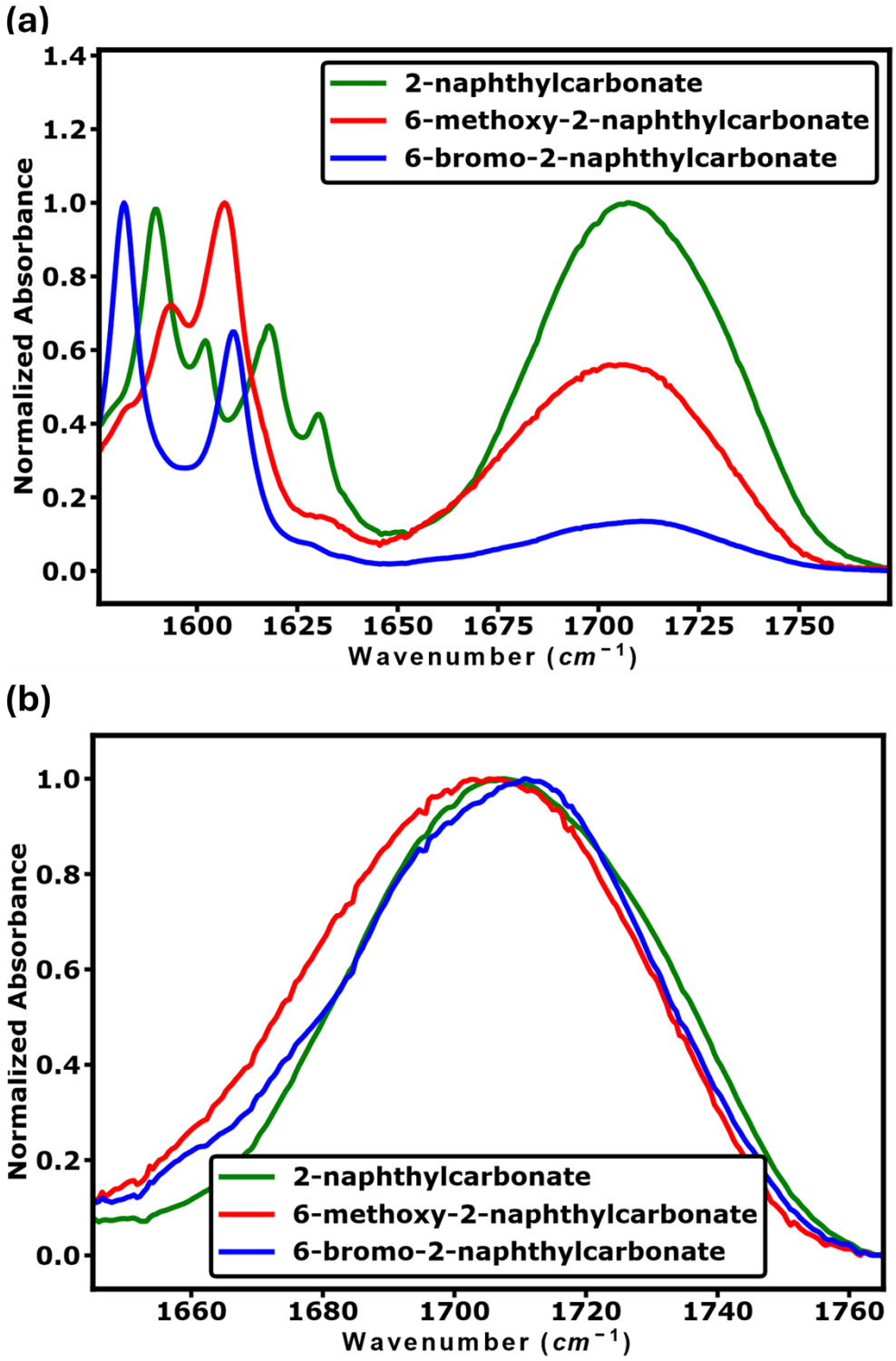

Figure S4. showing **(a)** FTIR spectra of 6-MeO-2-NpOCOO$^-$, 2-NpOCOO$^-$, and 6-Br-2-NpOCOO$^-$ (normalized to the ring modes). **(b)** Normalized FTIR peaks corresponding to the asymmetric carbonate stretching frequency for the same compounds.

Figure S4 (b) shows the FTIR spectrum of normalized asymmetric carbonate stretching frequency peaks of 6-Br-2-NpOCOO$^-$ (~1712 cm^{-1}), 2-NpOCOO$^-$ (~1707 cm^{-1}), and 6-MeO-2-NpOCOO$^-$ (~1702 cm^{-1}), which shows a progressive shift to lower frequency with increasing electron-donating character of the substituents. The -Br group is weakly electron-withdrawing which stabilizes the carbonate moiety through reduced electron density. It increases the C–O bond strength and its corresponding vibrational frequency. In contrast, the –OMe group donates electron density via resonance which weakens the C–O bonds in the carbonate by delocalizing negative charge, which results in a red shift of the asymmetric stretching mode. It is important to note that the carbonate frequency is very sensitive to its solvent environment. Therefore, we presented them as a blob in the figure below.

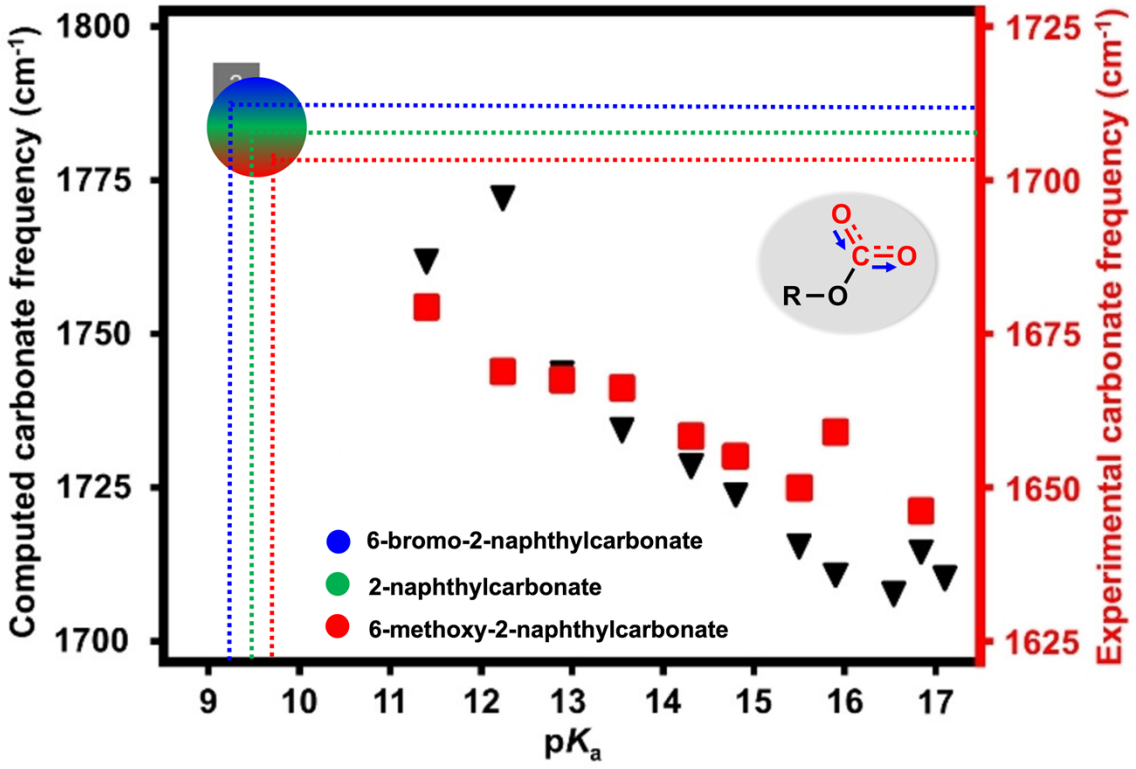

Figure S5. Figure showing the asymmetric stretching frequency of 6-Br-2-NpOCOO$^-$, 2-2-NpOCOO$^-$, and 6-MeO-2-NpOCOO$^-$ fits the trend of asymmetric carbonate frequency vs pK$_a$

The naphthol derivatives used in this study- 6-Br-2-NpOH (pK$_a$[13] = 9.26), 2-NpOH (pK$_a$[14] = 9.50), and 6-MeO-2-NpOH (pK$_a$[15] = 9.76), follow the trend we observed in our earlier work. As the acidity of the naphthols increases (i.e., lower pK$_a$), the carbonate vibrational frequencies shift to higher wavenumbers (blue shift).

Section S2.2: NMR assignments of 6-methoxy-2-naphthol species

For 6-MeO-2-NpOH: ^{1}H NMR (400 MHz, pure THF) δ 8.63 (s, 1H), 7.89 (d, *J* = 2.2 Hz, 1H), 7.62 (d, *J* = 8.7 Hz, 1H), 7.52 (d, *J* = 8.8 Hz, 1H), 7.40 (d, *J* = 8.8 Hz, 1H), 7.09 – 7.00 (m, 2H).

For 6-MeP-2-NpO^{-}: ^{1}H NMR (400 MHz, pure THF) δ 7.32 (d, *J* = 8.8 Hz, 1H), 7.19 (d, *J* = 9.0 Hz, 1H), 6.88 (s, 1H), 6.83 (d, *J* = 8.7 Hz, 1H), 6.76 (d, 1H), 6.67 (s, 1H).

Peak assignment to the 6-MeO-2-NpOCOO^{-} is not done due to the smeared nature of the spectra. Main features are at around 7.3 ppm and 6.95 ppm.

Section S2.3: Comments on blue shifted naphtholate peak in carbonate samples

In analyzing the emission spectrum of naphthylcarbonates samples, we note that the naphtholate emission in this sample appears as a shoulder and is significantly blue-shifted compared to pure naphtholate. In 2-NpOOCO^{-} emission data we observe a narrower emission associated with the pure naphtholate. We attribute this to the inner filter effect due to the highly concentrated sample. However, even in that sample a small shoulder that is blue shifted (around 400nm) is observed. This shoulder is more pronounced in 6-MeO-2-NpOCOO^{-} emission data presented in the main paper. We hypothesize two possible explainations for this. It may be that in the highly concentrated system naphtholates and naphthylcarbonates might be forming dimers. Which may be emitting in between canonical emission wavelenth of each of the species. It is also possible that the canonical naphtholate emission is burried for the methoxy subsituted sample under this feature and is not easily assigned in the spectrum. Another possible explaination could be that this blue shifted emission comes from naphthylcarbonate molecules that just released their CO_2 upon excitation but did not get the chance to assume their relaxed excited state conformation. It is expected that in these cases the emission will be blue shifted compared to canonical naphtholate emission which had the chance to fully relax before emitting. This hypothesis requires a very quick emission of the freshly formed naphtholate. We cannot prove either pathway without furthter experiments. However, since only the emission of naphthylcarbonate is required to construct the Förster cycle, the exact explaination of this emission feature is not needed and may be subject of a different study.

Section S2.4: Control Experiments

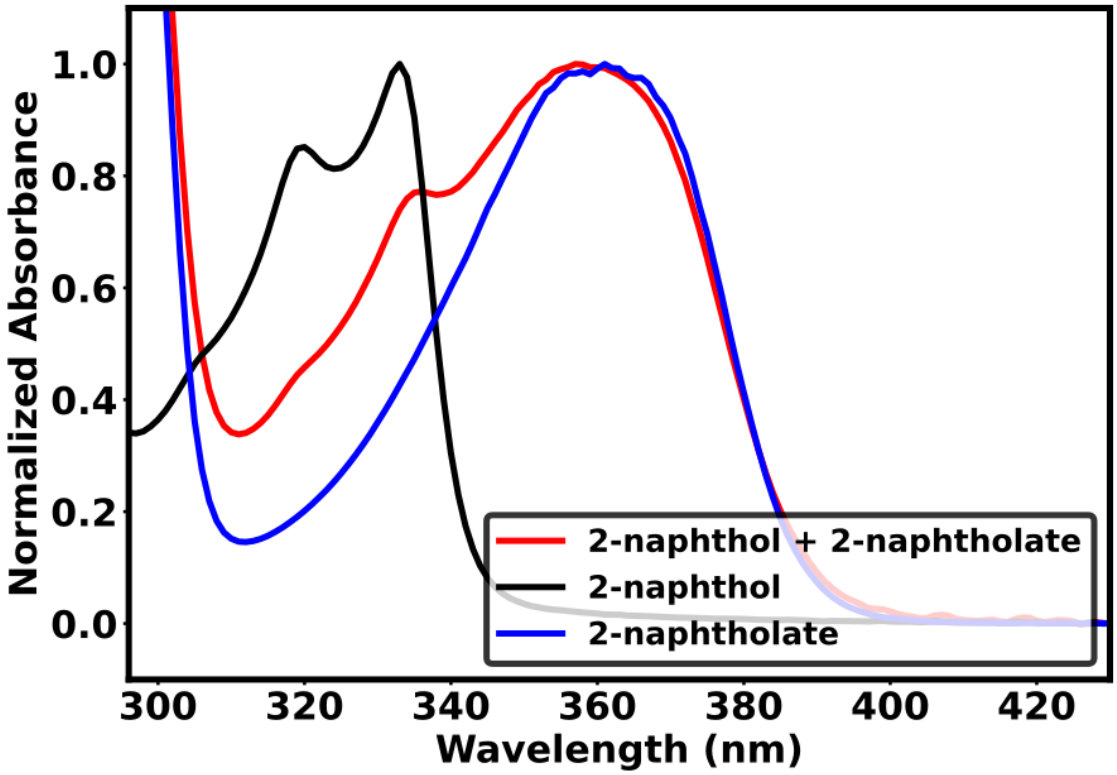

Figure S6 showing the Normalized UV-Vis absorption spectrum of 2-NpOH, 2-NpO$^-$, and 2-NpOH (25mM) and 2-NpO$^-$ (62.5mM) mixture.

As shown in Figure S6, the characteristic 2-NpO$^-$ peak is present in both the pure 2-NpO$^-$ spectrum and the 2-NpOCOO$^-$ spectrum, though in the latter it appears slightly shifted and broadened. To confirm that this effect is not unique to the carbonate formation, we prepared a 1:1 mixture of 25mM 2-NpOH and 62.5mM 2-NpO$^-$. The resulting UV-Vis absorption spectrum also shows a broadened and slightly shifted NpO$^-$ peak, supporting our interpretation that the spectral features are influenced by ion pairing and solution environment.

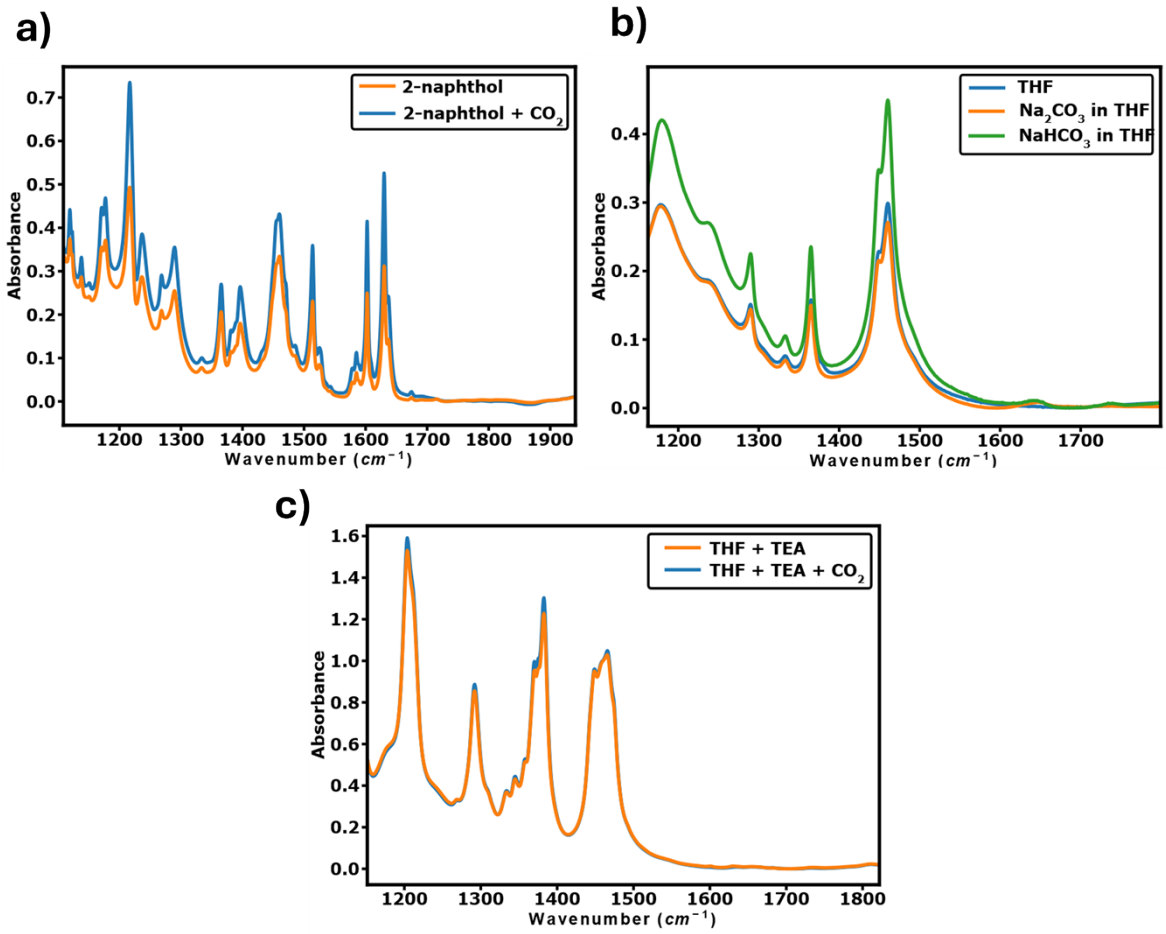

Figure S7. FTIR spectra of (a) 2-naphthol with CO_2 bubbling, (b) THF treated with Na_2CO_3 and $NaHCO_3$, and (c) THF–TEA mixture treated with CO_2. No significant changes are observed in any of the spectra.

When CO_2 is introduced to 2-naphthol, no carbonate is formed proving the need for the initial deprotonation step. Similarly, THF and TEA mixture, does not form any carbonates with CO_2 proving that there is no contamination in THF that can be forming the carbonates we observe in our experiments. The only distinct peak seen in the FTIR spectra is the dissolved CO_2 at 2349 cm^{-1} (not shown in the figures). Sodium carbonate (Na_2CO_3) and sodium bicarbonate ($NaHCO_3$) do not dissolve in THF, so no carbonate peak is seen in their FTIR spectra either proving that even with water contamination we could not be possibly observing their features as our carbonates.

Comments on Water Contamination

Ideally, CO_2 capture and release systems that are resilient to water are preferred. Water itself works as a CO_2 capture agent as well, forming various protonation stages of carbonic acid. In our work, we eliminated water as much as possible to prove the capture of CO_2 by the naphtholates and its subsequent photorelease. However, this does not imply that naphtholates and napthylcarbonates cannot form in aqueous media. If a naphtholate is introduced in aqueous media in the presence of CO_2, we suspect that both the Brønsted photoacid naphthol and the Lewis adduct naphthylcarbonate will form, given that naphtholate species can compete with water for carbonate formation. In that case, two channels for CO_2 photorelease are possible. The first channel will be release of proton from the naphthol and acidifying the medium, indirectly pushing the carbonate equilibrium towards release. The second channel would be the direct release of CO_2 from the naphthylcarbonate adduct, as discussed in this work. Dissecting these two pathways in aqueous media is likely to be challenging, because of ambiguities in the spectra of naphthylcarbonates and naphthols. We anticipate that further research will shed more light on this topic.

Section S3: Förster Cycle analysis

Section S3.1: Finding adiabatic transition energies

The adiabatic transition energies for 2-NpOH, 2-NpO^-, 2-$NpOCOO^-$, 6-Br-2-NpOH, 6-Br-2-NpO^-, 6-MeO-2-NpOH, 6-MeO-2-NpO^-, and 6-MeO-2-$NpOCOO^-$ were experimentally found. To calculate these energies, we have normalized both the absorption (solid lines) on emission (dashed lines) features of a given molecule. Next, we pinpointed where spectra intersected each other. The wavelength at which they intersect each other is an adequate estimate of the adiabatic energy as is often accepted by literature. The following are the spectra and analysis of all the species studied for this work.

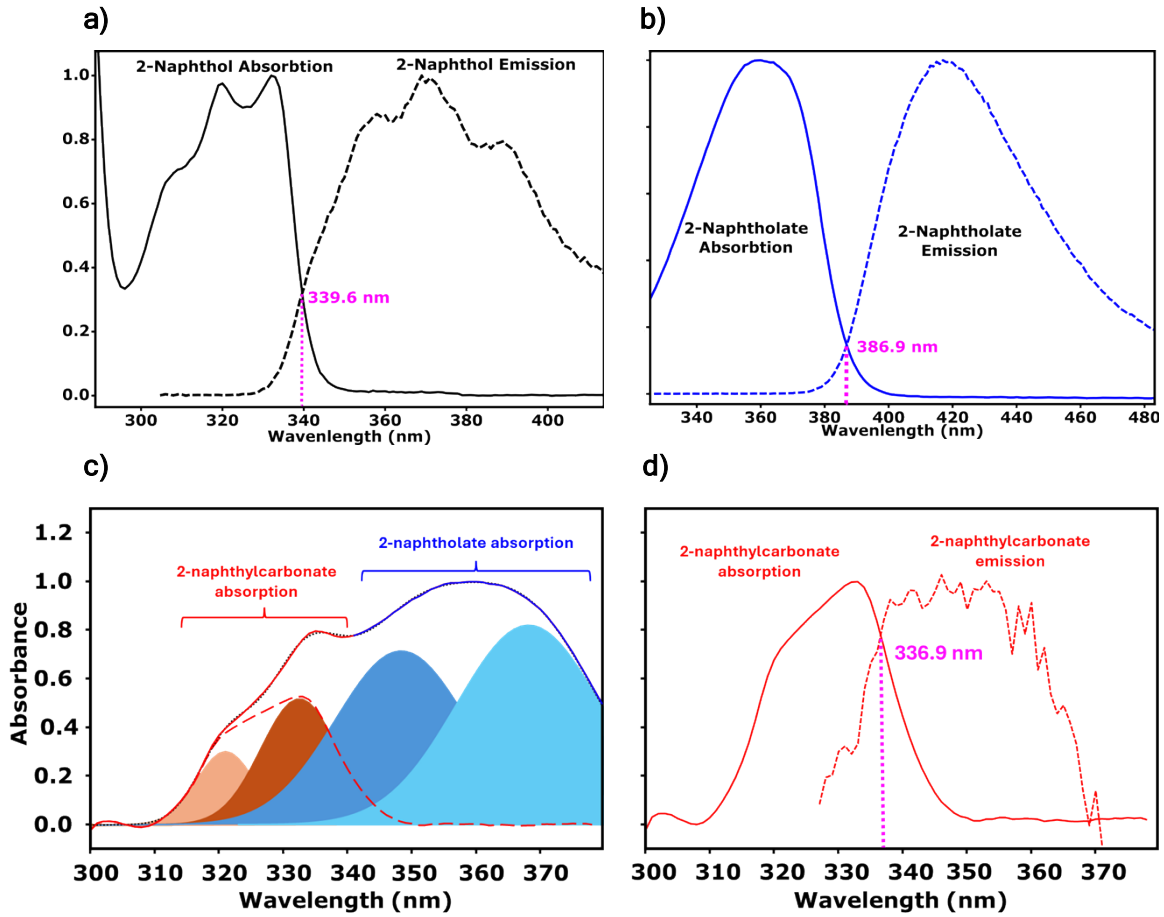

Figure S8. Figure showing the intersection points between the normalized absorption (solid lines) and normalized emission (dashed lines) for **(a)** 2-NpOH (black), **(b)** 2-NpO⁻ (blue), and **(d)** 2-NpOCOO⁻ (red). Converting the wavelength to eV the adiabatic transition energies for each species are 3.65, 3.20, and 3.68 eV respectively. In panel **(c)** baseline subtracted absorption of the 2-NpOCOO⁻ is shown. The solid red line corresponds with the absorption features associated with the carbonate while solid blue line corresponds with the unreacted naphtholate. Filled gaussian curves were used to explain the data and later utilized to remove the contribution of the naphtholate to yield the red dashed line. This line is used to find the adiabatic transition energy on panel d.

2-NpOCOO⁻ shows a very small emission intensity. This is likely due to the combination of inner filter effect, low initial carbonate concentration, and low quantum yield of the carbonate. Additionally, its absorption data is heavily contaminated with unreacted 2-NpO⁻. Both effects make it very challenging to find the exact crossing point of its absorption and emission data. In figure S8 (c), we have used a simple approach to estimate it which is sure to create a lot of

error in the final pK_a change we report in the excited state. However, as our computational results suggest, we are confident that we are still reporting a value that is a decent estimate of the real value.

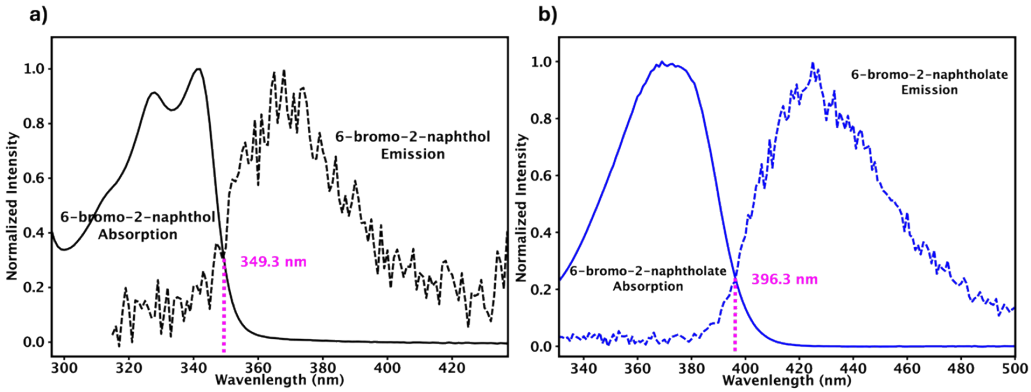

Figure S9. Figure showing the intersection points between the normalized absorption (solid lines) and normalized emission (dashed lines) for 6-Br-2-NpOH (black), 6-Br-2-NpO$^-$ (blue). Converting the wavelength to eV the adiabatic transition energies for each species are 3.13, and 3.55 respectively.

For 6-Br-2-NpOCOO$^-$ we only observed naphtholate emission. Therefore, we cannot calculate the excited state pK_a change for it.

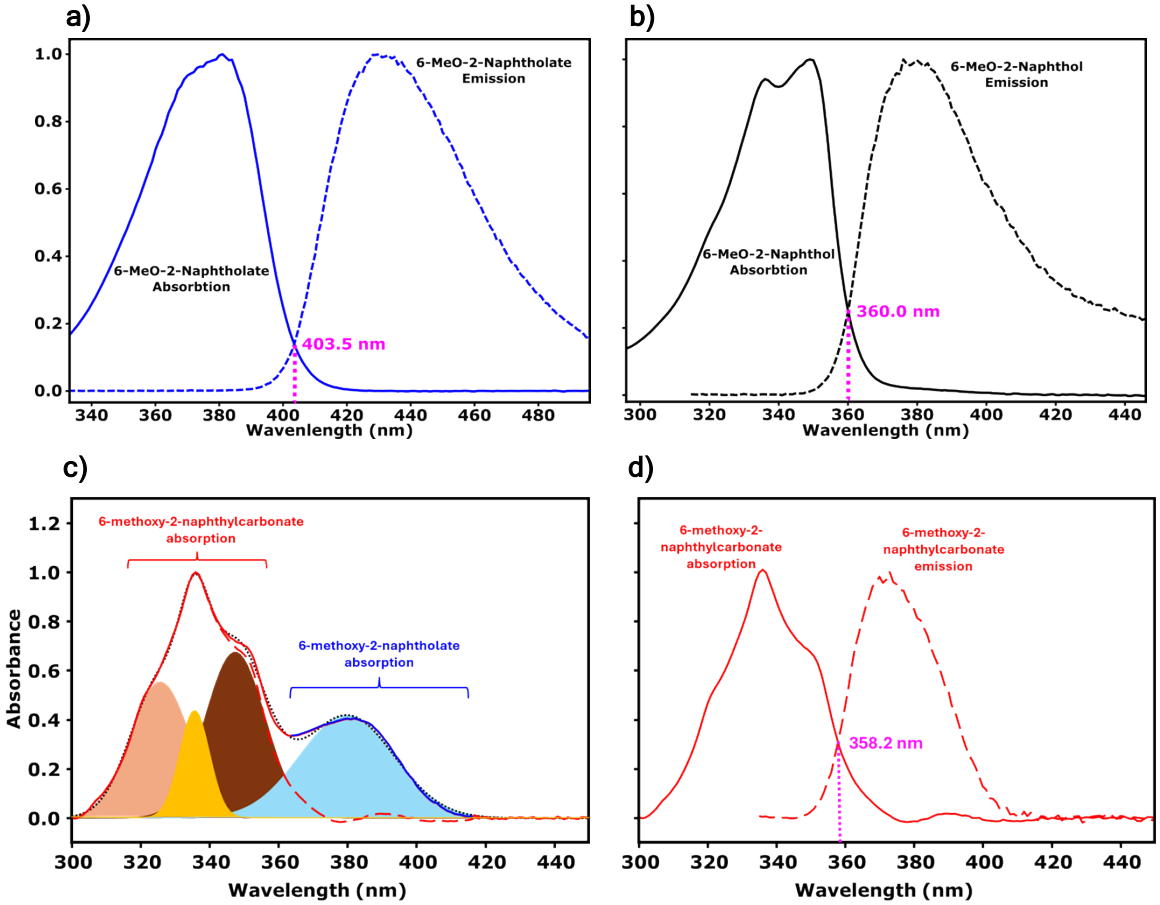

Figure S10. Figure showing the intersection points between the normalized absorption (solid lines) and normalized emission (dashed lines) for **(a)** 6-MeO-2-NpO$^-$ (black), **(b)** 6-MeO-2-NpO$^-$ (blue), and **(d)** 6-MeO-2-NpOCOO$^-$ (red). Blue part in the panel c notes the emission coming from the residual 6-MeO-2-NpO$^-$ present in the system. Emission feature coming from this naphtholate is further to the blue region and does not contribute in a meaningful manner to the result. Converting the wavelength to eV the adiabatic transition energies for each species are 3.07, 3.44, and 3.46 eV respectively. In panel **(c)** baseline subtracted absorption of the 6-MeO-2-NpOCOO$^-$ is shown. The solid red line corresponds with the absorption features associated with the carbonate while solid blue line corresponds with the unreacted naphtholate. Filled gaussian curves were used to explain the data and later utilized to remove the contribution of the naphtholate to yield the red dashed line. This line is used to find the adiabatic transition energy on panel d.

Section 3.2: Finding ΔpK_a for naphthols and ΔpK_{CO2} for naphthylcarbonates

We will be using the equation (1) presented in the main manuscript (reproduced here for convenience) to calculate the ΔpK_a and ΔpK_{CO2} values for all the species studied. It is important to note that these values have been reported to depend on the solvent the molecules are in and are only accurate for THF.

$$pK^{*}_{CO_2} - pK_{CO_2} = \Delta pK_{CO_2} = \frac{E_{00}^{base} - E_{00}^{acid}}{2.303RT}$$

Where E_{00} are the adiabatic transition energies, R is the gas constant, and T is the temperature. The temperature was taken to be 21 °C.

2-NpOH and 2-NpOCOO⁻:

$$\Delta pK_a = \frac{3.20 - 3.65}{2.303RT} = -7.71$$

$$\Delta pK_{CO_2} = \frac{3.20 - 3.68}{2.303RT} = -8.22$$

6-Br-2-NpOH:

$$\Delta pK_a = \frac{3.13 - 3.55}{2.303RT} = -7.19$$

6-MeO-2-NpOH and 6-MeO-2-NpOCOO⁻:

$$\Delta pK_a = \frac{3.07 - 3.44}{2.303RT} = -6.34$$

$$\Delta pK_{CO_2} = \frac{3.07 - 3.46}{2.303RT} = -6.68$$

We expect ΔpK_a values reported in this work are suscepitble to inaccurracies and we advise some caution when using the ΔpK_{CO_2} as absolute values. Due to the contamination from the naphtholate (especially significant in 2-naphthylcarbonate sample) accurate determination of

the adiabatic energies are challenging. While both experimental and computational results suggest that naphthols and naphthylcarbonates are expected to have similar drive for CO_2 release figuring out the small nuances in these energies are beyond our experimental capabilities. Although, very accurate $^{\Delta pK_{CO_2}}$ values cannot be determined we are confident that these values are very negative. Which proves that the molecules studied in this work are photoacidic and are suitable for reversible CO_2 captrue and release with light.

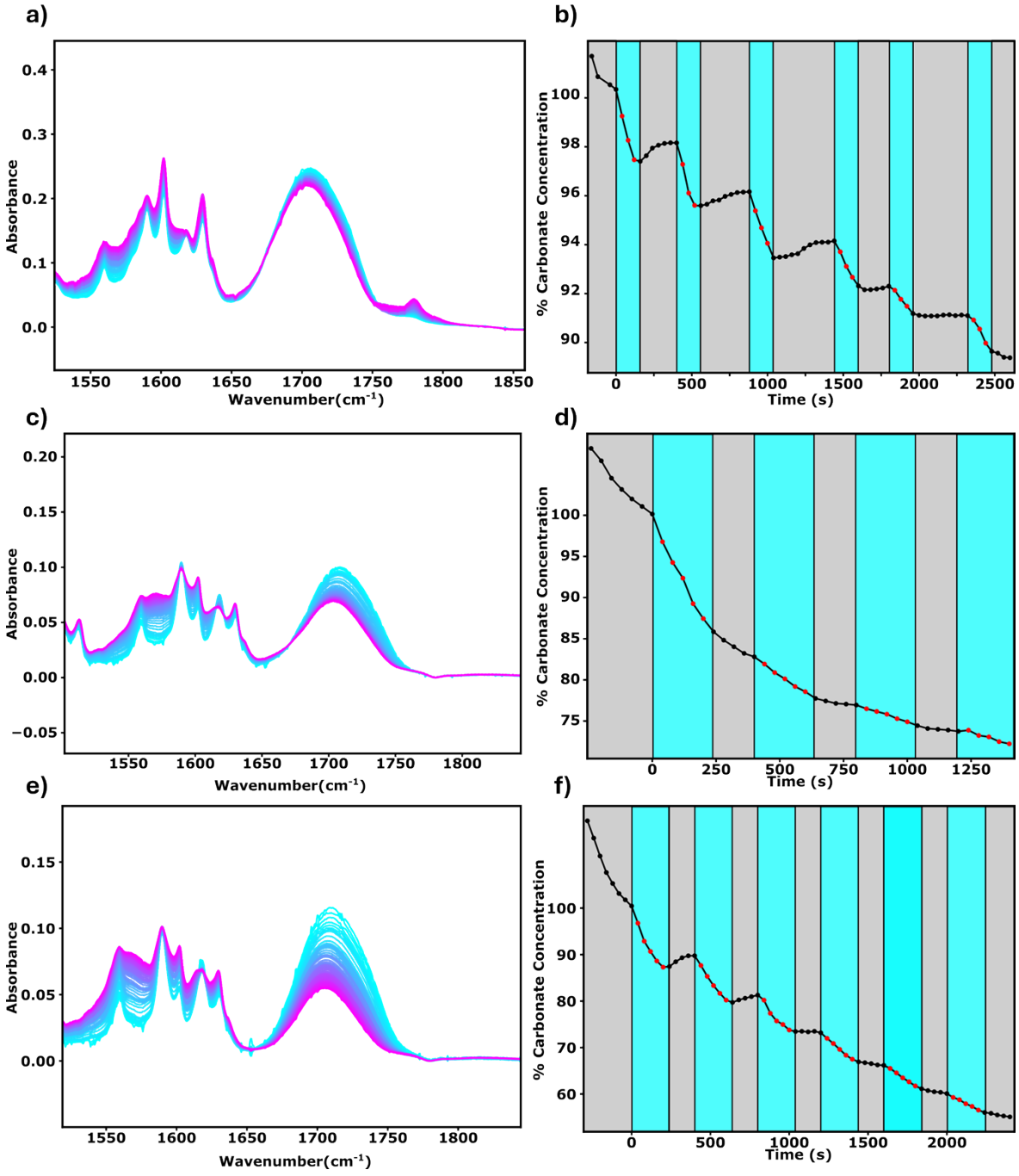

Figure S11: Data showing the spectral evolution of 2-NpOCOO⁻ as it is irradiated with light. The color scheme on the FTIR spectra (**a**, **c**, and **e**) notes the evolution of time (from cyan to purple). In the trace data (**b**, **d**, and **f**) cyan color notes where the light was shone and gray part was where the sample was left in the dark. Each trace data is coupled with the spectra to its left. Data pairs **a, b** and **e, f** are from samples with 10% (v/v) TEA in it, data pair **c, d** does not contain any TEA.

Section S4: Release data

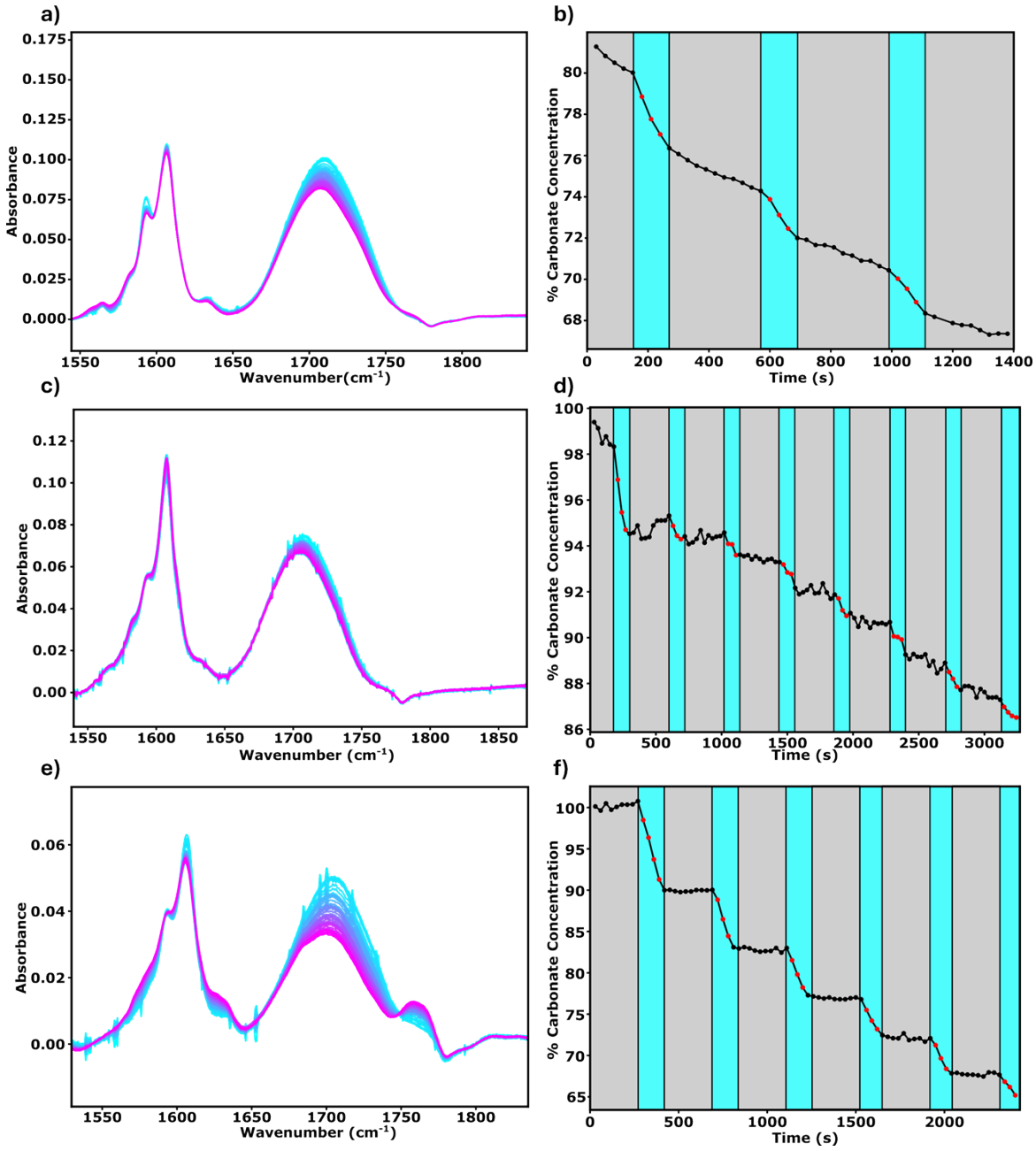

Figure S12. Data showing the spectral evolution of 6-MeO-2-NpOCOO⁻ as it is irradiated with light. The color scheme on the FTIR spectra (**a**, **c**, and **e**) notes the evolution of time (from cyan to purple). In the trace data (**b**, **d**, and **f**) cyan color notes where the light was shone and gray part was where the sample was left in the dark. Each trace data is coupled with the spectra to its left. Data pairs **a, b** and **e, f** are from samples with 10% (v/v) TEA in it, data pair **c, d** does not contain any TEA.

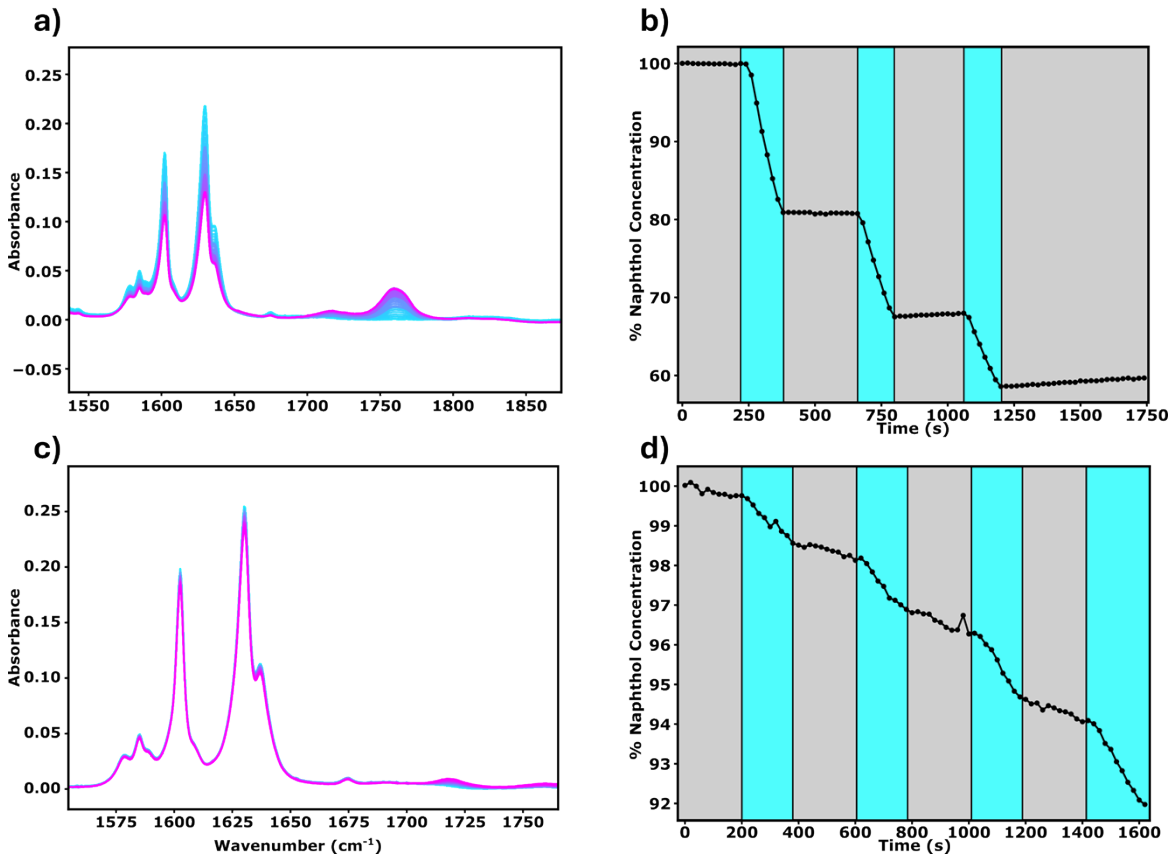

Figure S13. Data showing the spectral evolution of 2-NpOH as it is irradiated with light. The color scheme on the FTIR spectra (**a**, **c**) notes the evolution of time (from cyan to purple). In the trace data (**b**, **d**) cyan color notes where the light was shone and gray part was where the sample was left in the dark. Each trace data is coupled with the spectra to its left. Data pair **a, b** has 10% (v/v) TEA in it, data pair **c, d** does not contain any TEA.

Figure S11 and S12 examplifies the difficulty in achieving a stable system to collect reversible capture and release data. Unfortunately, water contamination and CO_2 leaving the system has drastic effects on the data. We have observed that addition of small amounts of TEA stabilizes the system and makes it more reversible. However, as it can be see in S13, TEA and naphthols react under 340 nm light to form a photoproduct. While the exact idendity of this product was not investigated further it is important to note that this product is indeed reversible as evidenced by the pick up of naphthol signal in figure S13 b at longer dark exposure. We have conducted this experiment many times and presented the most stable ones in this work. However, in all

of our experiments exposure of light triggered additional CO_2 release. A more advanced setup to quantitatively measure and test the reversibility of this system may be the subject of a further study.

Section S5: Computational results

Reaction Coordinate Diagrams for Ground-State CO_2 Capture

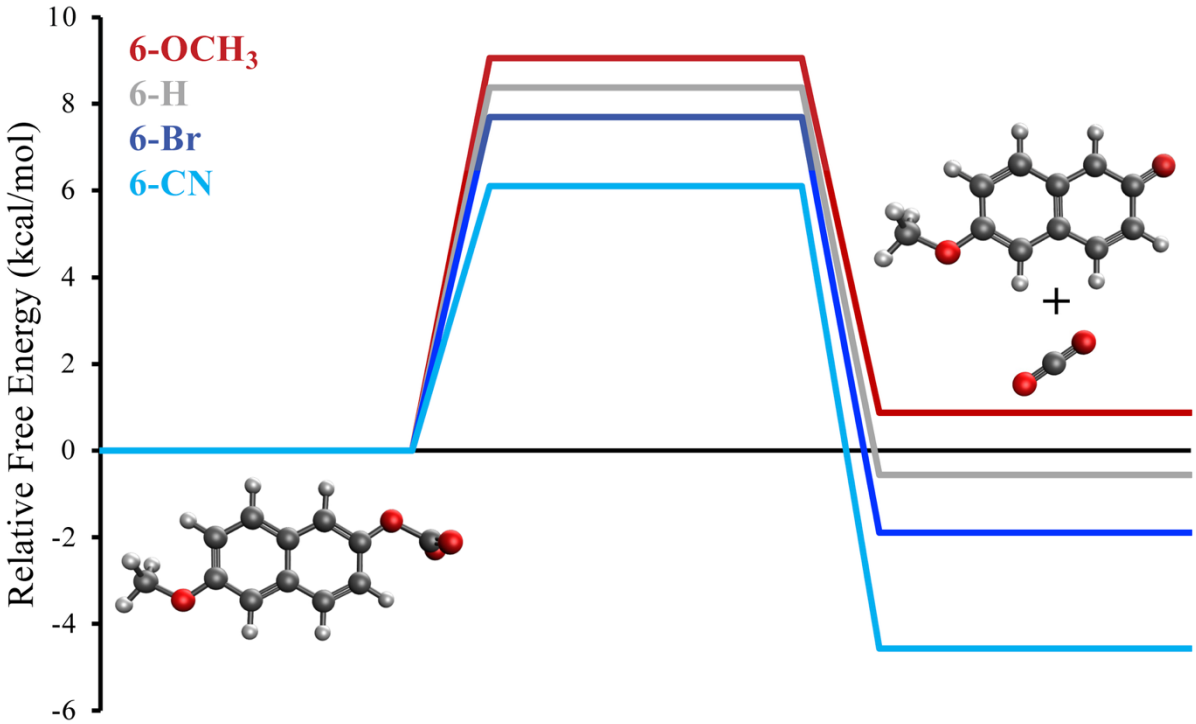

Figure S14: Ground state reaction coordinate diagram associated with thermal release of the CO_2 on the ground state for 2-naphthylcarbonate, 6-methoxy-2-naphthylcarbonate, 6-bromo-2-naphthylcarbonate, and 6-cyano-2-naphthylcarbonate. The calculations were performed at the ωB97M-V/def2-QZVPD//ωB97X-D/def2-SVPD level of theory with a polarizable continuum model (PCM) parametrized for THF. These calculations did not include the presence of a Na^+ ion.

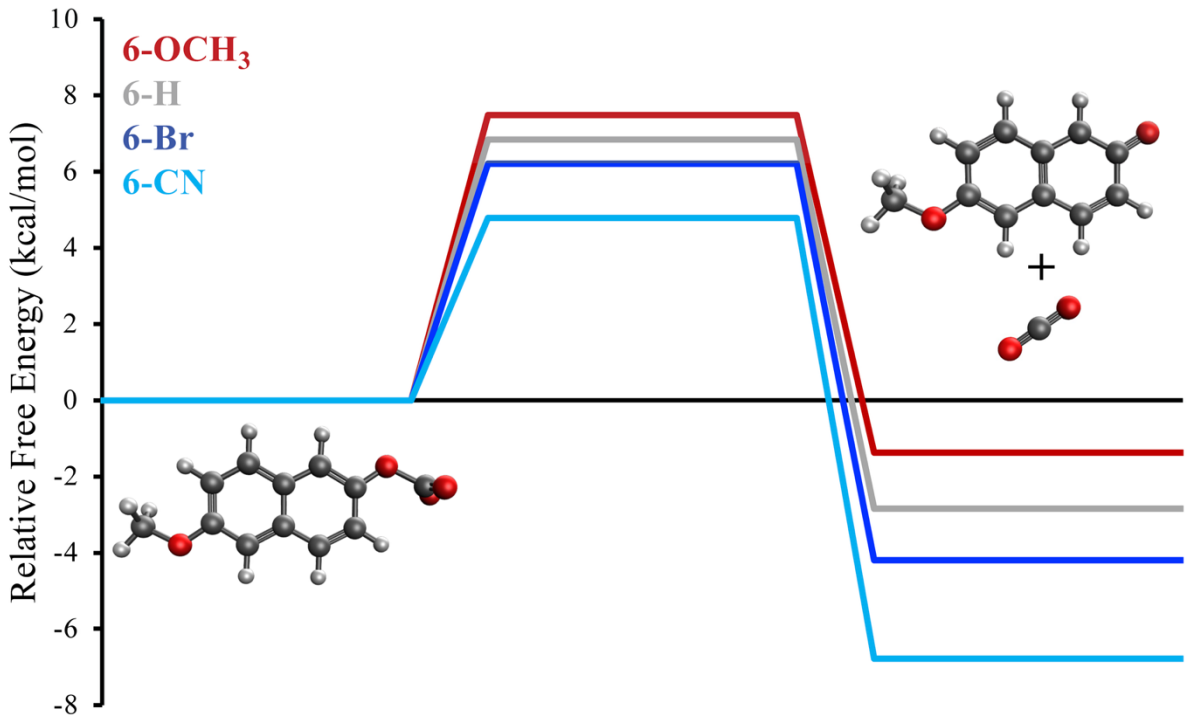

Figure S15: Ground state reaction coordinate diagram associated with thermal release of the CO_2 on the ground state for 2-naphthylcarbonate, 6-methoxy-2-naphthylcarbonate, 6-bromo-2-naphthylcarbonate, and 6-cyano-2-naphthylcarbonate. The calculations were performed at the ωB97M(2)/def2-QZVPPD//ωB97X-D/def2-SVPD level of theory with a PCM parametrized for THF. These calculations did not include the presence of a Na^+ ion.

Figure S14 shows the reaction coordinate diagram for the thermal release of CO_2 from all four 2-naphthylcarbonates considered in this study, calculated at the ωB97MV/def2-QZVPD//ωB97X-D/def2-SVPD level of theory. The diagram begins with the naphthylcarbonates, which we set to 0.0 kcal/mol relative free energy. For 6-methoxy-2-napthylcarbonate, CO_2 release involves a 9.06 kcal/mol barrier and is uphill in free energy by 0.88 kcal/mol. As the substituent becomes more electron-withdrawing, the release of CO_2 becomes more thermodynamically favorable, and the transition state barrier decreases. In particular, for 6-cyano-2-naphthylcarbonate, the transition state barrier and ΔG become 6.10 kcal/mol and -4.57 kcal/mol, respectively. This is consistent with the experimental observation that the spectral signatures of 6-methoxy-2-napthylcarbonate are significantly larger than those for 6-cyano-2-naphthylcarbonate.

Figure S15 repeats this analysis at the ωB97M(2)/def2-QZVPPD//ωB97X-D/def2-SVPD level of theory. In principle, this is a somewhat higher level of theory than that used in Figure S14. Now, CO_2 release from 6-methoxy-2-napthylcarbonate is calculated to be slightly exergonic with ΔG=-1.38 kcal/mol. As in Figure S14, the other 2-naphthylcarbonates exhibit more favorable kinetics and thermodynamics for CO_2 release, with ΔG=-4.57 kcal/mol for 6-cyano-2-napthylcarbonate

Figure S14 appears somewhat more consistent with experiment as it predicts a slightly thermodynamically stable 6-methoxy-2-napthylcarbonate complex. Furthermore, our calculations effectively report on ΔG under standard conditions. Even if 6-methoxy-2-napthylcarbonate is slightly unstable to CO_2 release under standard conditions, the non-standard conditions used in experiment likely shift the equilibrium towards adduct formation.

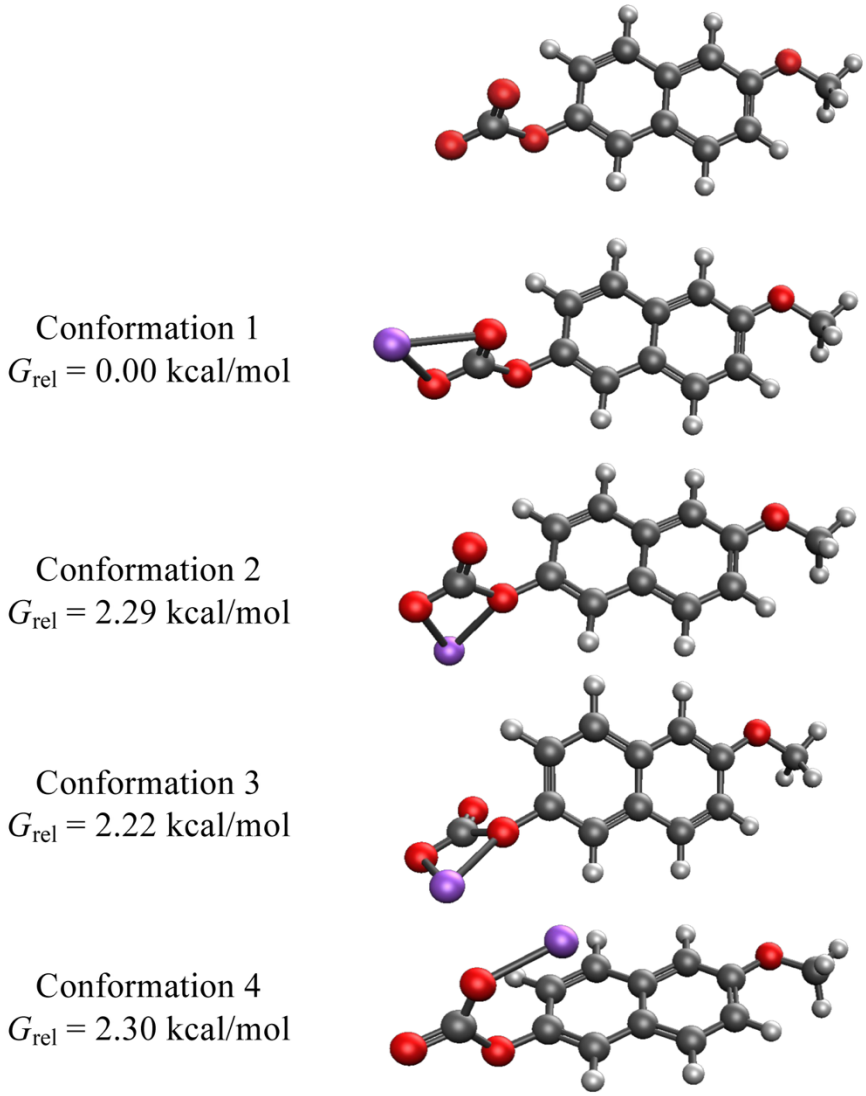

Figure S16: The ground state geometries of 6-methoxy-2-naphthylcarbonate and the contact ion pair between 6-methoxy-2-naphthylcarbonate and Na^+. The calculations were performed at the ωB97M-V/def2-QZVPD//ωB97X-D/def2-SVPD level of theory with a PCM parametrized for THF.

Conformation 1
G_{rel} = 0.64 kcal/mol

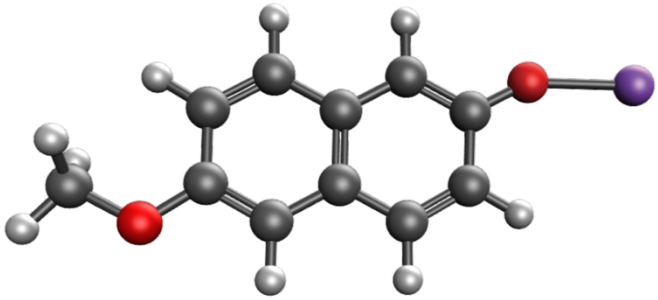

Conformation 2
G_{rel} = 0.00 kcal/mol

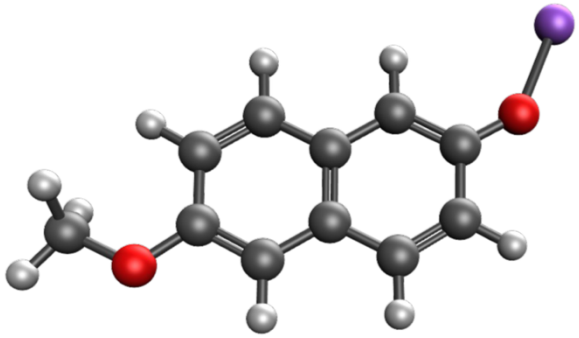

Figure S17: The ground state geometries of the contact ion pair between 6-methoxy-2-naphtholate and Na^+. The calculations were performed at the ωB97M-V/def2-QZVPD//ωB97X-D/def2-SVPD level of theory with a PCM parametrized for THF.

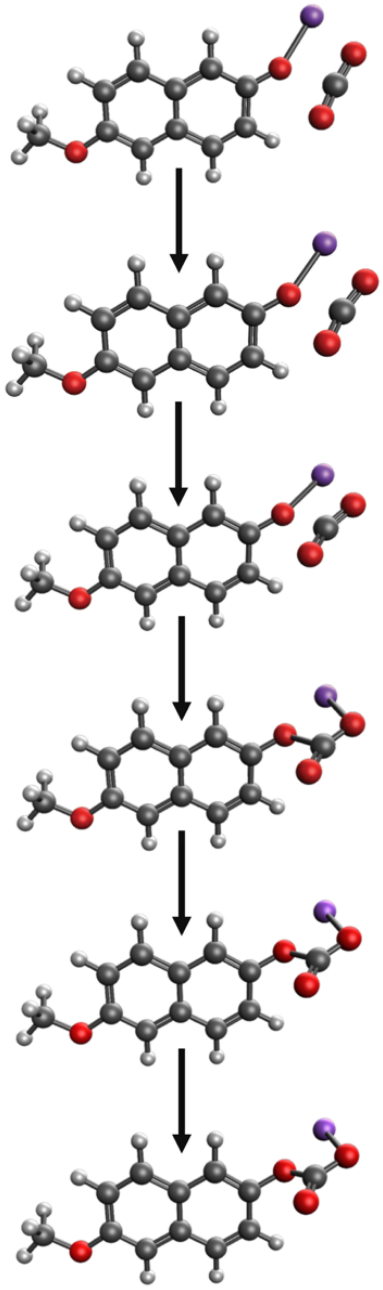

Figure S18: Representative geometries from a relaxed scan showing formation of conformation 2 of the 6-methoxy-2-naphthylcarbonate+Na^+ complex from CO_2 and the contact ion pair between 6-methoxy-2-naphtholate and Na^+. The relaxed scan was performed at the ωB97X-D/def2-SVPD level of theory with a PCM parametrized for THF.

As illustrated below, the electronic spectroscopy strongly supports the existence of contact ion pairs between the 2-naphtholates and Na^+. Figure S18 demonstrates a straightforward reaction coordinate through which CO_2 will add to such a contact ion pair. This will form either conformer 2 or 3 in Figure S16, which lie approximately 2.0 kcal/mol above the global minimum for the 6-methoxy-2-naphthylcarbonate+Na^+ complex. However, forming this global minimum geometry would require either the addition of CO_2 to bare 6-methoxy-2-naphtholate or a large rearrangement of the Na^+ in 6-methoxy-2-naphthylcarbonate+Na^+. As such, we

speculate that conformers 2 and 3 of 6-methoxy-2-naphthylcarbonate+Na^+ dominate in solution.

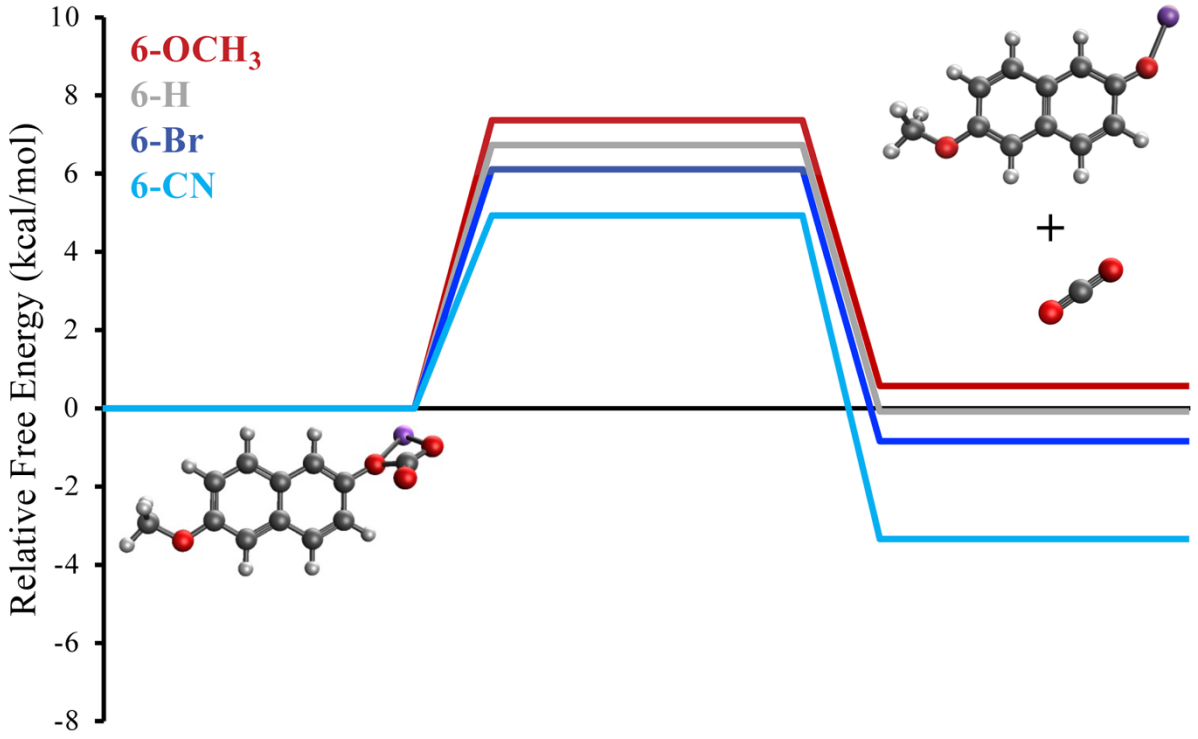

Figure S19: Ground state reaction coordinate diagram associated with thermal release of the CO_2 on the ground state for the contact ion pair between Na^+ and 2-naphthylcarbonate (gray), 6-methoxy-2-naphthylcarbonate (red), 6-bromo-2-naphthylcarbonate (dark blue), and 6-cyano-2-naphthylcarbonate (light blue). The calculations were performed at the ωB97M-V/def2-QZVPD//ωB97X-D/def2-SVPD level of theory with a polarizable continuum model parametrized for THF. The reaction coordinate diagrams involve the most stable conformation of the contact ion pair between Na^+ and the 2-naphtholates.

Figure S19 shows the reaction coordinate diagram for CO_2 release from the contact ion pair between Na^+ and the 2-naphthylcarbonates. As discussed above, we focus our analysis on the contact ion pair that can be formed without significant rearrangements of the Na^+. For 6-methoxy-2-naphthylcarbonate, the presence of the Na^+ ion does not significantly affect the transition state barrier but makes CO_2 release somewhat less thermodynamically unfavorable with ΔG=0.56 kcal/mol. As in Figure S14, electron-withdrawing substituents systematically lower the transition state barrier for CO_2 release and make the process more thermodynamically favorable. In particular, decomposition of 6-cyano-2-naphthylcarbonate+Na^+ is downhill in free energy by -3.34 kcal/mol.

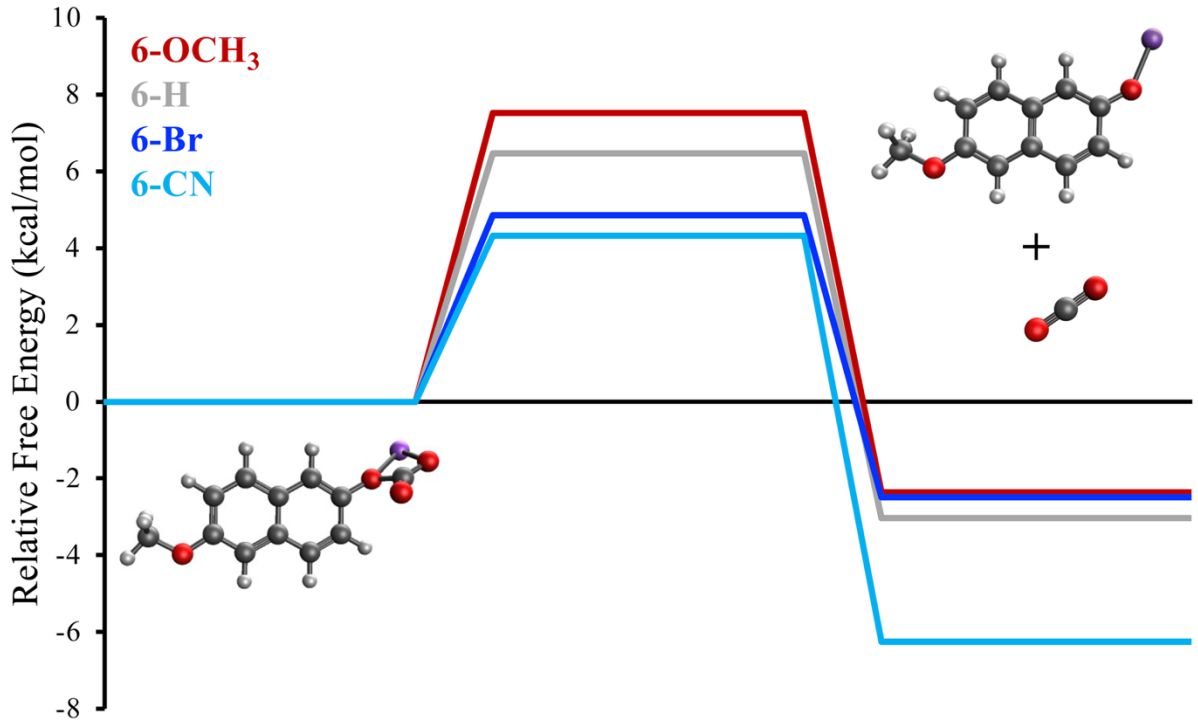

Figure S20: Ground state reaction coordinate diagram associated with thermal release of the CO_2 on the ground state for the contact ion pair between Na^+ and 2-naphthylcarbonate (gray), 6-methoxy-2-naphthylcarbonate (red), 6-bromo-2-naphthylcarbonate (dark blue), and 6-cyano-2-naphthylcarbonate (light blue). The calculations were performed at the ωB97M(2)/def2-QZVPPD//ωB97X-D/def2-SVPD level of theory with a polarizable continuum model parametrized for THF. The reaction coordinate diagrams involve the most stable conformation of the contact ion pair between Na^+ and the 2-naphtholates.

As above, we explored how the reaction coordinate diagram in Figure S19 changes when calculated at the ωB97M(2)/def2-QZVPPD//ωB97X-D/def2-SVPD level of theory. As in Figure S15, 6-methoxy-2-naphthylcarbonate is slightly thermodynamically unstable at this level of theory, with CO_2 release downhill in free energy by -2.36 kcal/mol. Interestingly, the thermodynamics of CO_2 release no longer exhibit a systematic trend at this level of theory. Because of both of these observations, we posit that the ωB97MV/def2-QZVPD//ωB97X-D/def2-SVPD level of theory provides a more realistic description of ground state CO_2 capture in these systems.

Summarizing the Relative Free Energies of Conformers

Table S1: Summary of the relative populations of the two conformers of the 2-naphthols, which differ by the relative orientation of the hydroxyl group.[a]

	Relative Free Energy Conformer 1 (kcal/mol)	Relative Free Energy Conformer 2 (kcal/mol)	Relative Thermal Population Conformer 1	Relative Thermal Population Conformer 2
6-MeO-2-NpOH	0.00	0.24	59.83%	40.17%
2-NpOH	0.18	0.00	42.57%	57.43%
6-Br-2-NpOH	0.16	0.00	43.11%	56.89%

[a]Calculations performed at the ωB97M-V/def2-QZVPD//ωB97X-D/def2-SVPD level of theory with a polarizable continuum model parameterized for THF. The free energy and relative thermal populations were evaluated at T=298.15 K.

Table S2: Summary of the relative populations of the two conformers of the contact ion pair between Na+ and the 2-naphtholates, which differ by the relative orientation of the Na^+ as shown in Figure S16.[a]

	Relative Free Energy Conformer 1 (kcal/mol)	Relative Free Energy Conformer 2 (kcal/mol)	Relative Thermal Population Conformer 1	Relative Thermal Population Conformer 2
6-MeO-2-NpO$^-$+Na$^+$	0.64	0.00	25.32%	74.68%
2-NpO$^-$+Na$^+$	0.41	0.00	33.32%	66.68%
6-Br-2-NpO$^-$+Na$^+$	0.17	0.00	42.97%	57.03%

[a]Calculations performed at the ωB97M-V/def2-QZVPD//ωB97X-D/def2-SVPD level of theory with a polarizable continuum model parameterized for THF. The free energy and relative thermal populations were evaluated at T=298.15 K.

Table S3: Summary of the relative free energies of the conformers of the contact ion pair between Na^+ and the 2-naphthylcarbonates shown in Figure S16.[a,b]

	Relative Free Energy (kcal/mol)
6-MeO-2-NpOCOO$^-$+Na$^+$	
Conformer 1	-2.22
Conformer 2	0.07
Conformer 3	0.00
Conformer 4	0.08
2-NpOCOO$^-$+Na$^+$	
Conformer 1	-2.21
Conformer 2	0.12
Conformer 3	0.00
Conformer 4	0.40
6-Br-2-NpOCOO$^-$+Na$^+$	
Conformer 1	-2.30
Conformer 2	0.12
Conformer 3	0.00
Conformer 4	1.09

[a]Calculations performed at the ωB97M-V/def2-QZVPD//ωB97X-D/def2-SVPD level of theory with a polarizable continuum model parameterized for THF. The free energy and relative thermal populations were evaluated at T=298.15 K.

[b]Based on the reaction pathway shown in Figure S18 as well as spectroscopic analysis below, we do not believe that the 2-naphthylcarbonate+Na^+ contact ion pairs reach thermal equilibrium under experimental conditions. We believe that the conformers 2 and 3 dominate over conformer 1 under experimental conditions.

Harmonic Vibrational Analysis

Table S4: Harmonic vibrational frequency analysis of key modes of 6-MeO-2-NpO$^-$ with and without forming a contact ion pair with Na^+.[a]

	Ring Mode 1[b]	**Ringe Mode 2[b]**	**Ringe Mode 3[b]**	**Ringe Mode 4[b]**
6-MeO-2-NpO$^-$	1693.79 (1)	1652.85 (543)	1609.78 (334)	1538.85 (12)
6-MeO-2-NpO$^-$+Na$^+$ Conformer 1[c]	1701.12 (1)	1660.38 (566)	1622.22 (184)	1546.42 (49)
6-MeO-2-NpO$^-$+Na$^+$ Conformer 2[c]	1700.89 (1)	1660.39 (548)	1622.66 (187)	1546.67 (52)
6-MeO-2-NpO$^-$+Na$^+$[d]	1700.95 (1)	1660.39 (553)	1622.55 (186)	1546.61 (51)

[a]Harmonic vibrational frequencies calculated at the ωB97X-D/def2-TZVPPD with a PCM parameterized for THF.
[b]Harmonic vibrational frequencies are reported in $cm^{-1,}$ and their intensities are stated in parentheses.
[c]Conformers differ based on the relative orientation of the Na^+ as shown in Figure S17.
[d]Thermal average of the 2 conformers with Boltzmann weights evaluated at room temperature at the ωB97M-V/def2-QZVPD//ωB97X-D/def2-SVPD level of theory.

Table S4 summarizes the harmonic vibrational frequencies of the ring modes of 6-MeO-2-NpO$^-$ with and without forming a contact ion pair with Na^+. These normal modes are dominated by C-H wagging and C-C stretching motions in the aromatic ring system. Ring mode 2 also contains some C-O stretching character. We note that the presence of the Na+ ion weakly perturbs the harmonic vibrational frequencies and normal mode vibrational motions.

Table S5: Harmonic vibrational frequency analysis of key modes of 6-MeO-2-NpOCOO$^-$ with and without forming a contact ion pair with Na^+.[a]

	Relative Free Energy (kcal/mol)	Bright Ring Mode (cm^{-1})	Carbonate Mode (cm^{-1})	Scaled Carbonate Mode (cm^{-1})[b]	Error in Scaled Carbonate Mode (cm^{-1})[c]
6-MeO-2-NpOCOO$^-$		1676.94	1742.89	1671.24	-30.76
6-MeO-2-NpOCOO$^-$ + Na^+ Conf 1[d]	0.00	1681.85	1671.58	1598.18	-103.82
6-MeO-2-NpOCOO$^-$ + Na^+ Conf 2[d]	2.00	1679.02	1794.20	1718.31	16.31
6-MeO-2-NpOCOO$^-$ + Na^+ Conf 3[d]	1.94	1678.73	1794.81	1719.19	17.19
6-MeO-2-NpOCOO$^-$ + Na^+ Conf 4[d]	2.02	1673.29	1761.18	1692.46	-9.54

[a]Harmonic vibrational frequencies calculated at the ωB97X-D/def2-TZVPPD with a PCM parameterized for THF.
[b]The harmonic scaling factor is based on the bright ring mode found in the experimental spectrum around 1608 cm^{-1}. The scaling factor is approximately 0.96 for all of these species.
[c]Based on the experimental position of the carbonate stretch of 1702 cm^{-1}.
[d]The conformations differ based on the position of the Na+ ion: see Figure S16.

Table S5 summarizes the carbonate stretching vibrational mode and the highest frequency bright ring mode of 6-MeO-2-NpOCOO$^-$ with and without forming a contact ion pair with Na^+. As for 6-MeO-2-NpO$^-$, the harmonic vibrational frequency of the ring mode is only weakly affected by the presence of the Na^+ ion. In contrast, the position of the carbonate stretch is strongly modulated by the presence and position of the Na^+. Indeed, for the contact ion pair, the position of this vibrational mode varies over 120 cm^{-1} based on how the Na^+ is bound to the 6-MeO-2-NpOCOO$^-$. We speculate that this could explain some of the spectral breadth observed in the experimental spectrum for the peak assigned to the carbonate mode.

As expected, the harmonic vibrational frequencies overestimate the experimental peak positions because of their absence of anharmonicity. We found that a harmonic scaling factor of approximately 0.96 shifts the calculated bright ring mode into good agreement with the experimental peak position at 1608 cm^{-1}. Applying this scaling factor to the carbonate stretching vibrational mode led to the scaled carbonate modes in Table S5. The difference between these scaled carbonate modes and the experimental center of the carbonate stretching peak, 1702 cm^{-1}, is given in the final column.

The scaled carbonate stretch modes for conformations 2-4 of the contact ion pair between 6-MeO-2-NpOCOO$^-$ and Na^+ are all in better agreement with the experimental peak position than bare 6-MeO-2-NpOCOO$^-$. Moreover, as discussed in Figure S18, conformations 2 and 3 are directly formed from CO_2 binding to the contact ion pair between 6-MeO-2-NpO$^-$ and Na^+. The scaled carbonate stretch of conformation 1 is over 100 cm^{-1} lower than the experimental peak, providing additional evidence that this structure is likely less relevant under experimental conditions. While this analysis cannot definitively prove that contact ion pairs dominate the

experimental reaction mixture, Table S5 strongly suggests that they significantly contribute to the experimental spectrum.

Table S6: Key harmonic vibrational frequencies of 6-methoxy-2-naphthol, 6-methoxy-2-naphtholate, and 6-methoxy-2-naphthylcarbonate.[a]

	Carbonate Mode[b]	Ring Mode 1[b]	Ring Mode 2[b]	Ring Mode 3[b]	Ring Mode 4[b]
6-MeO-2-NpOH Conformer 1[c]		1714.11 (2)	1677.22 (422)	1650.80 (2)	1576.78 (147)
6-MeO-2-NpOH Conformer 2[c]		1719.38 (7)	1684.34 (324)	1648.32 (12)	1569.68 (260)
6-MeO-2-NpOH[d]		1716.23 (4)	1680.08 (382)	1649.80 (6)	1573.93 (193)
6-MeO-2-NpO$^-$+Na$^+$[d]		1700.95 (1)	1660.39 (553)	1622.55 (186)	1546.61 (51)
6-MeO-2-NpO$^-$		1693.79 (1)	1652.85 (543)	1609.78 (334)	1538.85 (12)
6-MeO-2-NpOCOO$^-$ + Na$^+$ Conf 3[e]	1794.81 (1120)	1714.76 (17)	1678.73 (280)	1646.25 (2)	1564.80 (154)
6-MeO-2-NpOCOO$^-$ + Na$^+$ Conf 4[e]	1761.18 (1395)	1708.33 (14)	1673.29 (424)	1639.15 (7)	1559.61 (187)
6-MeO-2-NpOCOO$^-$	1742.89 (1314)	1713.14 (11)	1676.94 (403)	1644.69 (10)	1564.22 (141)

[a]Harmonic vibrational frequencies calculated at the ωB97X-D/def2-TZVPPD with a PCM parameterized for THF.
[b]Harmonic vibrational frequencies reported in cm^{-1} with their intensities stated in parentheses.
[c]Conformers differ based on the relative orientation of the hydroxyl group.
[d]Thermal average of the 2 conformers with Boltzmann weights evaluated at room temperature at the ωB97M-V/def2-QZVPD//ωB97X-D/def2-SVPD level of theory.
[e]The conformations differ based on the position of the Na+ ion: see Figure S16.

Table S6 summarizes the calculated harmonic vibrational frequencies for 6-methoxy-2-naphthol, 6-methoxy-2-naphtholate, and 6-methoxy-2-naphthylcarbonate, where the anions are described both with and without a Na^+ ion. Focusing on the highest frequency bright ring mode, the thermally averaged harmonic frequency for 6-methoxy-naphthol is 1680.08 cm^{-1}. The comparable mode for 6-methoxy-naptholate is red-shifted by 19.69-27.23 cm^{-1}, depending on whether or not a strongly interacting Na^+ is present. In contrast, for 6-methoxy-2-naphthylcarbonate, the ring mode is within 1.35-6.79 cm^{-1} of the harmonic vibrational frequency of 6-methoxy-naphthol. This agrees with the experimental observation that the 6-methoxy-naphthol and 6-methoxy-2-naphthylcarbonate ring modes have remarkably similar positions in the IR spectrum.

Table S7: Harmonic vibrational frequency analysis of key modes of 2-NpO$^-$ with and without forming a contact ion pair with Na^+.[a]

	Ring Mode 1[b]	Ring Mode 2[b]	Ring Mode 3[b]	Ring Mode 4[b]
2-NpO$^-$	1675.91 (202)	1650.43 (370)	1609.35 (240)	1539.81 (137)
2-NpO$^-$+Na$^+$ Conformer 1[c]	1686.14 (202)	1658.12 (317)	1622.15 (123)	1547.28 (143)
2-NpO$^-$+Na$^+$ Conformer 2[c]	1685.81 (203)	1658.02 (298)	1622.48 (124)	1547.21 (139)
2-NpO$^-$+Na^{+d}	1685.92 (203)	1658.06 (304)	1622.37 (124)	1547.24 (140)

[a]Harmonic vibrational frequencies calculated at the ωB97X-D/def2-TZVPPD with a PCM parameterized for THF.
[b]Harmonic vibrational frequencies are reported in $cm^{-1,}$ and their intensities are stated in parentheses.
[c]Conformers differ based on the relative orientation of the Na^+ as shown in Figure S17.
[d]Thermal average of the 2 conformers with Boltzmann weights evaluated at room temperature at the ωB97M-V/def2-QZVPD//ωB97X-D/def2-SVPD level of theory.

Table S8: Harmonic vibrational frequency analysis of key modes of 6-Br-2-NpO$^-$ with and without forming a contact ion pair with Na^+.[a]

	Ring Mode 1[b]	Ring Mode 2[b]	Ring Mode 3[b]	Ring Mode 4[b]
6-Br-2-NpO$^-$	1664.98 (236)	1645.48 (406)	1602.90 (322)	1526.29 (451)
6-Br-2-NpO$^-$+Na$^+$ Conformer 1[c]	1677.39 (221)	1651.83 (381)	1616.97 (168)	1535.17 (333)
6-Br-2-NpO$^-$+Na$^+$ Conformer 2[c]	1677.16 (222)	1651.62 (359)	1617.21 (168)	1534.91 (325)
6-Br-2-NpO$^-$+Na^{+d}	1677.26 (222)	1651.71 (368)	1617.11 (168)	1535.02 (328)

[a]Harmonic vibrational frequencies calculated at the ωB97X-D/def2-TZVPPD with a PCM parameterized for THF.
[b]Harmonic vibrational frequencies are reported in $cm^{-1,}$ and their intensities are stated in parentheses.
[c]Conformers differ based on the relative orientation of the Na^+ as shown in Figure S17.
[d]Thermal average of the 2 conformers with Boltzmann weights evaluated at room temperature at the ωB97M-V/def2-QZVPD//ωB97X-D/def2-SVPD level of theory.

Table S9: Key harmonic vibrational frequencies of 2-naphthol, 2-naphtholate, and 2-naphthylcarbonate.[a]

	Carbonate Mode[b]	Ring Mode 1[b]	Ring Mode 2[b]	Ring Mode 3[b]	Ring Mode 4[b]
2-NpOH Conformer 1[c]		1712.68 (164)	1680.32 (27)	1650.80 (22)	1569.86 (120)
2-NpOH Conformer 2[c]		1705.94 (171)	1673.77 (92)	1653.79 (7)	1579.46 (59)
2-NpOH[d]		1708.81 (168)	1679.56 (65)	1652.52 (14)	1575.37 (85)
2-NpO$^-$+Na$^+$[d]		1685.92 (203)	1658.06 (304)	1622.37 (124)	1547.24 (140)
2-NpO$^-$		1675.91 (202)	1650.43 (370)	1609.35 (240)	1539.81 (137)
2-NpOCOO$^-$ + Na$^+$ Conf 3[e]	1798.86 (1123)	1711.05 (46)	1674.52 (32)	1650.11 (4)	1566.30 (41)
2-NpOCOO$^-$ + Na$^+$ Conf 4[e]	1765.13 (1375)	1704.59 (104)	1670.29 (113)	1643.84 (6)	1561.09 (69)
2-NpOCOO$^-$	1746.72 (1293)	1706.64 (154)	1672.11 (82)	1647.12 (5)	1563.52 (50)

[a]Harmonic vibrational frequencies calculated at the ωB97X-D/def2-TZVPPD with a PCM parameterized for THF.
[b]Harmonic vibrational frequencies reported in cm^{-1} with their intensities stated in parentheses.
[c]Conformers differ based on the relative orientation of the hydroxyl group.
[d]Thermal average of the 2 conformers with Boltzmann weights evaluated at room temperature at the ωB97M-V/def2-QZVPD//ωB97X-D/def2-SVPD level of theory.
[e]The conformations differ based on the position of the Na+ ion: see Figure S16.

Table S10: Key harmonic vibrational frequencies of 6-bromo-2-naphthol, 6-bromo-2-naphtholate, and 6-bromo-2-naphthylcarbonate.[a]

	Carbonate Mode[b]	Ring Mode 1[b]	Ring Mode 2[b]	Ring Mode 3[b]	Ring Mode 4[b]
6-Br-2-NpOH Conformer 1[c]		1710.57 (135)	1668.88 (94)	1647.88 (31)	1560.43 (193)
6-Br-2-NpOH Conformer 2[c]		1702.76 (142)	1663.25 (195)	1651.67 (2)	1572.51 (95)
6-Br-2-NpOH[d]		1706.13 (139)	1665.68 (151)	1650.03 (15)	1567.30 (137)
6-Br-2-NpO$^-$+Na$^+$[d]		1677.26 (222)	1651.71 (368)	1617.11 (168)	1535.02 (328)
2-NpO$^-$		1664.98 (236)	1645.48 (406)	1602.90 (322)	1526.29 (451)
6-Br-2-NpOCOO$^-$ + Na$^+$ Conf 3[e]	1802.85 (1128)	1707.75 (22)	1663.53 (125)	1646.98 (0)	1555.75 (74)
6-Br-2-NpOCOO$^-$ + Na$^+$ Conf 4[e]	1768.81 (1414)	1699.93 (61)	1661.09 (232)	1640.08 (1)	1549.93 (113)
6-Br-2-NpOCOO$^-$	1753.28 (1327)	1702.46 (112)	1661.29 (181)	1644.21 (4)	1553.10 (92)

[a]Harmonic vibrational frequencies calculated at the ωB97X-D/def2-TZVPPD with a PCM parameterized for THF.
[b]Harmonic vibrational frequencies reported in cm^{-1} with their intensities stated in parentheses.
[c]Conformers differ based on the relative orientation of the hydroxyl group.
[d]Thermal average of the 2 conformers with Boltzmann weights evaluated at room temperature at the ωB97M-V/def2-QZVPD//ωB97X-D/def2-SVPD level of theory.
[e]The conformations differ based on the position of the Na+ ion: see Figure S16.

Electronic Spectroscopy

Table S11: Vertical excitation and emission energies for the $S_0 \rightarrow S_1$ and $S_0 \rightarrow S_2$ transitions of 6-methoxy-2-naphthol, 6-methoxy-2-naphtholate, and 6-methoxy-2-naphthylcarbonate with and without a contact ion pair with Na^+.

	Vertical Excitation Energy $S_0 \rightarrow S_1$ (eV)[a,b]	**Vertical Excitation Energy $S_0 \rightarrow S_2$ (eV)[a,b]**	**Vertical Emission Energy $S_1 \rightarrow S_0$ (eV)[b,c]**	**Vertical Emission Energy $S_2 \rightarrow S_0$ (eV)[b,c]**
6-MeO-2-NpOH Conformer 1[d]	3.82 (0.067)	4.81 (0.046)	3.40 (0.079)	4.49 (0.026)
6-MeO-2-NpOH Conformer 2[d]	3.78 (0.068)	4.79 (0.049)	3.37 (0.080)	4.47 (0.028)
6-MeO-2-NpOH[e]	3.81 (0.067)	4.80 (0.047)	3.38 (0.080)	4.48 (0.027)
6-MeO-2-NpO$^-$	2.88 (0.076)	3.82 (0.0005)	2.50 (0.069)	3.14 (0.00007)
6-MeO-2-NpO$^-$+Na$^+$ Conformer 1[f]	3.23 (0.076)	3.27 (0.002)	2.81 (0.074)	3.06 (0.0009)
6-MeO-2-NpO$^-$+Na$^+$ Conformer 2[f]	3.24 (0.079)	3.24 (0.007)	2.84 (0.078)	3.08 (0.0004)
6-MeO-2-NpO$^-$+Na$^+$[e]	3.24 (0.078)	3.24 (0.001)	2.83 (0.077)	3.08 (0.0005)
6-MeO-2-NpOCOO$^-$	3.95 (0.056)	4.76 (0.060)	3.17 (0.083)	4.42 (0.061)
6-MeO-2-NpOCOO$^-$+Na$^+$ Conformer 1[g]	3.99 (0.052)	4.74 (0.060)	3.53 (0.074)	4.39 (0.040)
6-MeO-2-NpOCOO$^-$+Na$^+$ Conformer 2[g]	3.99 (0.051)	4.72 (0.064)	3.51 (0.072)	4.36 (0.033)
6-MeO-2-NpOCOO$^-$+Na$^+$ Conformer 3[g]	3.99 (0.051)	4.72 (0.064)	3.51 (0.072)	4.36 (0.034)
6-MeO-2-NpOCOO$^-$+Na$^+$ Conformer 4[g]	3.90 (0.054)	4.65 (0.079)	3.42 (0.073)	4.32 0.032)

[a]Calculations performed at the ADC(2)/def2-TZVPD//ωB97X-D/def2-SVPD level of theory with a PCM parameterized for THF. The resolution of identity approximation was used to accelerate the ADC(2) calculations.
[b]Oscillator strength of the transition given in parenthesis.
[c]Excited state geometry optimizations performed using ROKS-ωB97X-D/def2-SVPD.
[d]Conformers differ based on the relative orientation of the hydroxyl group.
[e]Thermal average of the 2 conformers with Boltzmann weights evaluated at room temperature at the ωB97M-V/def2-QZVPD//ωB97X-D/def2-SVPD level of theory.
[f]Conformers differ based on the relative orientation of the Na^+.
[g]Conformers are shown in Figure S16.

Table S11 summarizes the vertical transitions of 6-MeO-2-NpOH, 6-MeO-2-2NpO$^-$, and 6-MeO-2-2NpOCOO$^-$. For the anions, we considered the possibility of both bare ions and contact ion pairs with Na^+. We see that the calculated $S_0 \rightarrow S_1$ absorption and $S_1 \rightarrow S_0$ emission transitions of 6-MeO-2-2NpO$^-$ and 6-MeO-2-2NpO$^-$+Na^+ are significantly red-shifted relative to 6-MeO-2-NpOH, consistent with experiment. In contrast, the vertical transitions of 6-MeO-2-2NpOCOO$^-$ and 6-MeO-2-2NpOCOO$^-$+Na^+ are much more similar to those of 6-MeO-2-NpOH. This agrees qualitatively with the experimental spectra.

Table S12: Adiabatic $S_0 \rightarrow S_1$ energy gaps for 6-methoxy-2-naphthol, 6-methoxy-2-naphtholate, and 6-methoxy-2-naphthylcarbonate with and without a contact ion pair with Na^+.

	Adiabatic $S_0 \rightarrow S_1$ Energy Gap (eV)[a,b]	**Adiabatic $S_0 \rightarrow S_1$ Energy Gap with ZPE (eV)[a,b]**
6-MeO-2-NpOH Conformer 1[c]	3.63	3.52
6-MeO-2-NpOH Conformer 2[c]	3.59	3.49
6-MeO-2-NpOH[d]	3.61	3.51
6-MeO-2-NpO$^-$	2.73	2.62
6-MeO-2-NpO$^-$+Na^+ Conformer 1[e]	3.05	2.95
6-MeO-2-NpO$^-$+Na^+ Conformer 2[e]	3.06	2.96
6-MeO-2-NpO$^-$+Na^+[d]	3.06	2.96
6-MeO-2-NpOCOO$^-$	3.55	3.43
6-MeO-2-NpOCOO$^-$+Na^+ Conformer 1[f]	3.80	3.69
6-MeO-2-NpOCOO$^-$+Na^+ Conformer 2[f]	3.78	3.66
6-MeO-2-NpOCOO$^-$+Na^+ Conformer 3[f]	3.77	3.66
6-MeO-2-NpOCOO$^-$+Na^+ Conformer 4[f]	3.69	3.57

[a]Calculations performed at the ADC(2)/def2-TZVPD//ωB97X-D/def2-SVPD level of theory with a PCM parameterized for THF. The resolution of identity approximation was used to accelerate the ADC(2) calculations.
[b]Excited state geometry optimizations performed using ROKS-ωB97X-D/def2-SVPD.
[c]Conformers differ based on the relative orientation of the hydroxyl group.
[d]Thermal average of the 2 conformers with Boltzmann weights evaluated at room temperature at the ωB97M-V/def2-QZVPD//ωB97X-D/def2-SVPD level of theory.
[e]Conformers differ based on the relative orientation of the Na^+.
[f]Conformers are shown in Figure S16.

Table S13: Vertical excitation and emission energies for the $S_0 \rightarrow S_1$ and $S_0 \rightarrow S_2$ transitions of 2-naphthol, 2-naphtholate, and 2-naphthylcarbonate with and without a contact ion pair with Na^+.

	Vertical Excitation Energy $S_0 \rightarrow S_1$ (eV)[a,b]	**Vertical Excitation Energy $S_0 \rightarrow S_2$ (eV)[a,b]**	**Vertical Emission Energy $S_1 \rightarrow S_0$ (eV)[b,c]**	**Vertical Emission Energy $S_2 \rightarrow S_0$ (eV)[b,c]**
2-NpOH Conformer 1[d]	4.16 (0.036)	4.78 (0.046)	3.73 (0.065)	4.36 (0.030)
2-NpOH Conformer 2[d]	4.20 (0.033)	4.82 (0.045)	3.77 (0.063)	4.37 (0.031)
2-NpOH[e]	4.19 (0.035)	4.80 (0.045)	3.75 (0.064)	4.36 (0.031)
2-NpO$^-$	3.10 (0.077)	3.55 (0.0001)	2.67 (0.066)	3.20 (0.0001)
2-NpO$^-$+Na$^+$ Conformer 1[f]	3.47 (0.069)	3.46 (0.002)	3.00 (0.067)	3.26 (0.001)
2-NpO$^-$+Na$^+$ Conformer 2[f]	3.48 (0.074)	3.44 (0.001)	3.04 (0.072)	3.29 (0.0004)
2-NpO$^-$+Na$^+$[e]	3.48 (0.072)	3.44 (0.001)	3.02 (0.070)	3.28 (0.001)
2-NpOCOO$^-$	4.31 (0.014)	4.78 (0.067)	3.39 (0.072)	4.31 (0.044)
2-NpOCOO$^-$+Na$^+$ Conformer 1[g]	4.39 (0.006)	4.83 (0.074)	3.85 (0.060)	4.28 (0.042)
2-NpOCOO$^-$+Na$^+$ Conformer 2[g]	4.39 (0.005)	4.82 (0.075)	3.93 (0.051)	4.25 (0.040)
2-NpOCOO$^-$+Na$^+$ Conformer 3[g]	4.39 (0.005)	4.82 (0.075)	3.93 (0.052)	4.25 (0.040)
2-NpOCOO$^-$+Na$^+$ Conformer 4[g]	4.37 (0.009)	4.77 (0.065)	3.94 (0.064)	4.22 (0.025)

[a]Calculations performed at the ADC(2)/def2-TZVPD//ωB97X-D/def2-SVPD level of theory with a PCM parameterized for THF. The resolution of identity approximation was used to accelerate the ADC(2) calculations.
[b]Oscillator strength of the transition given in parenthesis.
[c]Excited state geometry optimizations performed using ROKS-ωB97X-D/def2-SVPD.
[d]Conformers differ based on the relative orientation of the hydroxyl group.
[e]Thermal average of the 2 conformers with Boltzmann weights evaluated at room temperature at the ωB97M-V/def2-QZVPD//ωB97X-D/def2-SVPD level of theory.
[f]Conformers differ based on the relative orientation of the Na^+.
[g]Conformers are shown in Figure S16.

Table S14: Adiabatic $S_0 \rightarrow S_1$ energy gaps for 2-naphthol, 2-naphtholate, and 2-naphthylcarbonate with and without a contact ion pair with Na^+.

	Adiabatic $S_0 \rightarrow S_1$ Energy Gap (eV)[a,b]	**Adiabatic $S_0 \rightarrow S_1$ Energy Gap with ZPE (eV)[a,b]**
2-NpOH Conformer 1[c]	4.01	3.89
2-NpOH Conformer 2[c]	4.06	3.93
2-NpOH[d]	4.04	3.92
2-NpO$^-$	2.93	2.81
2-NpO$^-$+Na$^+$ Conformer 1[e]	3.29	3.19
2-NpO$^-$+Na$^+$ Conformer 2[e]	3.30	3.20
2-NpO$^-$+Na$^+$[d]	3.29	3.19
2-NpOCOO$^-$	3.81	3.67
2-NpOCOO$^-$+Na$^+$ Conformer 1[f]	4.23	4.10
2-NpOCOO$^-$+Na$^+$ Conformer 2[f]	4.24	4.11
2-NpOCOO$^-$+Na$^+$ Conformer 3[f]	4.24	4.11
2-NpOCOO$^-$+Na$^+$ Conformer 4[f]	4.26	4.13

[a]Calculations performed at the ADC(2)/def2-TZVPD//ωB97X-D/def2-SVPD level of theory with a PCM parameterized for THF. The resolution of identity approximation was used to accelerate the ADC(2) calculations.
[b]Excited state geometry optimizations performed using ROKS-ωB97X-D/def2-SVPD.
[c]Conformers differ based on the relative orientation of the hydroxyl group.
[d]Thermal average of the 2 conformers with Boltzmann weights evaluated at room temperature at the ωB97M-V/def2-QZVPD//ωB97X-D/def2-SVPD level of theory.
[e]Conformers differ based on the relative orientation of the Na^+.
[f]Conformers are shown in Figure S16.

Table S15: Vertical excitation and emission energies for the $S_0 \rightarrow S_1$ and $S_0 \rightarrow S_2$ transitions of 6-bromo-2-naphthol, 6-bromo-2-naphtholate, and 6-bromo-2-naphthylcarbonate with and without a contact ion pair with Na^+.

	Vertical Excitation Energy $S_0 \rightarrow S_1$ (eV)[a,b]	**Vertical Excitation Energy $S_0 \rightarrow S_2$ (eV)[a,b]**	**Vertical Emission Energy $S_1 \rightarrow S_0$ (eV)[b,c]**	**Vertical Emission Energy $S_2 \rightarrow S_0$ (eV)[b,c]**
6-Br-2-NpOH Conformer 1[d]	4.03 (0.037)	4.70 (0.067)	3.60 (0.060)	4.32 (0.035)
6- Br -NpOH Conformer 2[d]	4.07 (0.035)	4.73 (0.065)	3.64 (0.058)	4.34 (0.034)
6- Br -NpOH[e]	4.06 (0.035)	4.72 (0.066)	3.62 (0.059)	4.33 (0.034)
6- Br -2-NpO$^-$	2.96 (0.079)	3.39 (0.00001)	2.53 (0.063)	3.04 (0.00005)
6- Br -2-NpO$^-$+Na$^+$ Conformer 1[f]	3.34 (0.071)	3.56 (0.002)	2.88 (0.066)	3.37 (0.001)
6- Br -2-NpO$^-$+Na$^+$ Conformer 2[f]	3.34 (0.076)	3.53 (0.001)	2.90 (0.070)	3.39 (0.0005)
6- Br -2-NpO$^-$+Na$^+$[e]	3.34 (0.074)	3.54 (0.001)	2.89 (0.068)	3.38 (0.001)
6- Br -2-NpOCOO$^-$	4.18 (0.018)	4.67 (0.080)	3.22 (0.071)	4.20 (0.090)
6- Br -2-NpOCOO$^-$+Na$^+$ Conformer 1[g]	4.27 (0.009)	4.76 (0.073)		
6- Br -2-NpOCOO$^-$+Na$^+$ Conformer 2[g]	4.26 (0.008)	4.75 (0.075)	3.75 (0.046)	4.24 (0.040)
6- Br -2-NpOCOO$^-$+Na$^+$ Conformer 3[g]	4.26 (0.008)	4.75 (0.076)	3.75 (0.046)	4.24 (0.040)
6- Br -2-NpOCOO$^-$+Na$^+$ Conformer 4[g]				

[a]Calculations performed at the ADC(2)/def2-TZVPD//ωB97X-D/def2-SVPD level of theory with a PCM parameterized for THF. The resolution of identity approximation was used to accelerate the ADC(2) calculations.
[b]Oscillator strength of the transition given in parenthesis.
[c]Excited state geometry optimizations performed using ROKS-ωB97X-D/def2-SVPD.
[d]Conformers differ based on the relative orientation of the hydroxyl group.
[e]Thermal average of the 2 conformers with Boltzmann weights evaluated at room temperature at the ωB97M-V/def2-QZVPD//ωB97X-D/def2-SVPD level of theory.
[f]Conformers differ based on the relative orientation of the Na^+.
[g]Conformers are shown in Figure S16.

Table S16: Adiabatic $S_0 \rightarrow S_1$ energy gaps for 6-bromo-2-naphthol, 6-bromo-2-naphtholate, and 6-bromo-2-naphthylcarbonate with and without a contact ion pair with Na^+.

	Adiabatic $S_0 \rightarrow S_1$ Energy Gap (eV)[a,b]	**Adiabatic $S_0 \rightarrow S_1$ Energy Gap with ZPE (eV)[a,b]**
6-Br-2-NpOH Conformer 1[c]	3.87	3.75
6-Br-2-NpOH Conformer 2[c]	3.91	3.79
6-Br-2-NpOH[d]	3.89	3.77
6-Br-2-NpO$^-$	2.79	2.67
6-Br-2-NpO$^-$+Na$^+$ Conformer 1[e]	3.15	3.02
6-Br-2-NpO$^-$+Na$^+$ Conformer 2[e]	3.16	3.03
6-Br-2-NpO$^-$+Na$^+$[d]	3.16	3.03
6-Br-2-NpOCOO$^-$	3.65	3.50
6-Br-2-NpOCOO$^-$+Na$^+$ Conformer 1[f]		
6-Br-2-NpOCOO$^-$+Na$^+$ Conformer 2[f]	4.06	3.92
6-Br-2-NpOCOO$^-$+Na$^+$ Conformer 3[f]	4.06	3.93
6-Br-2-NpOCOO$^-$+Na$^+$ Conformer 4[f]		

[a]Calculations performed at the ADC(2)/def2-TZVPD//ωB97X-D/def2-SVPD level of theory with a PCM parameterized for THF. The resolution of identity approximation was used to accelerate the ADC(2) calculations.
[b]Excited state geometry optimizations performed using ROKS-ωB97X-D/def2-SVPD.
[c]Conformers differ based on the relative orientation of the hydroxyl group.
[d]Thermal average of the 2 conformers with Boltzmann weights evaluated at room temperature at the ωB97M-V/def2-QZVPD//ωB97X-D/def2-SVPD level of theory.
[e]Conformers differ based on the relative orientation of the Na^+.
[f]Conformers are shown in Figure S16.

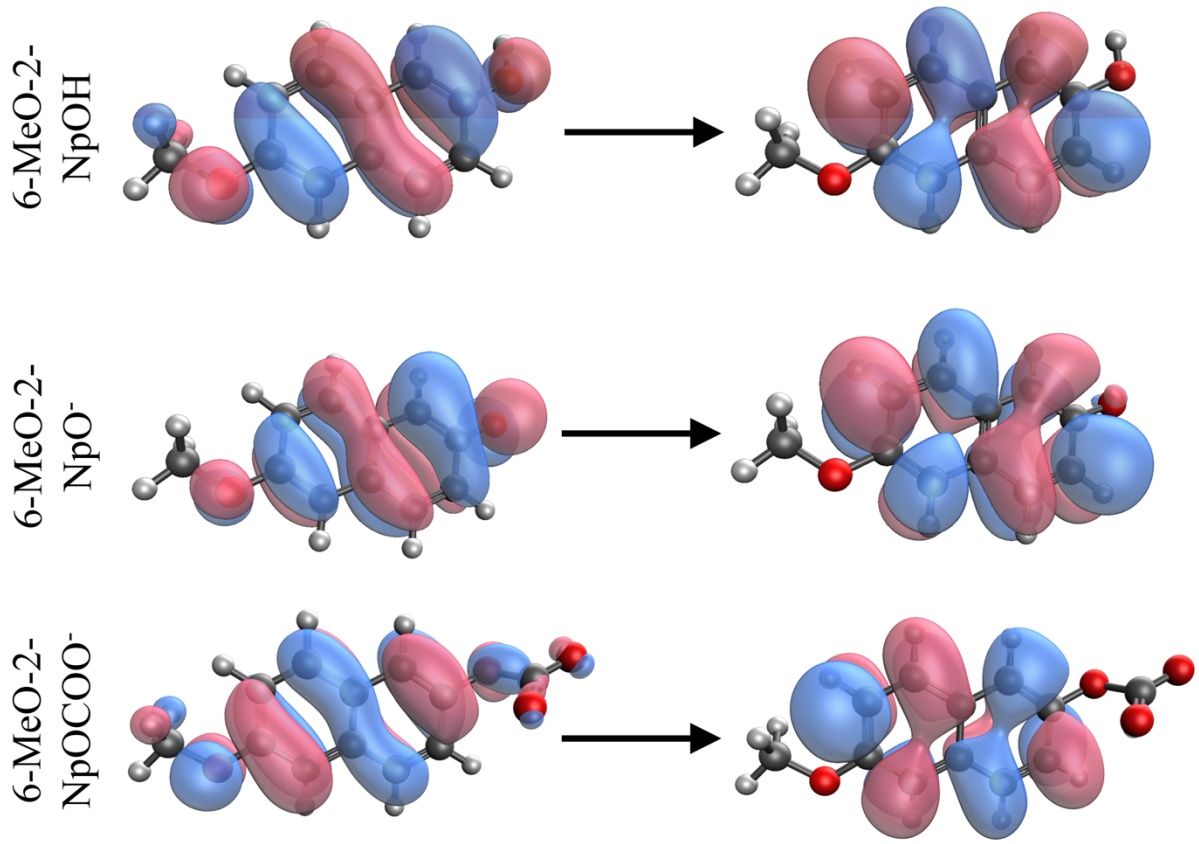

Figure S21: The natural transition orbitals (NTOs) for the $S_0 \rightarrow S_1$ transition of 6-MeO-2-NpOH, 6-MeO-2-NpO^-, and 6-MeO-2-$NpOCOO^-$. The NTOs were calculated at the ADC(2)/def2-tzvpd//ROKS-ωB97X-D/def2-SVPD level of theory at the ground state optimized geometry and plotted with an isovalue of 0.06.

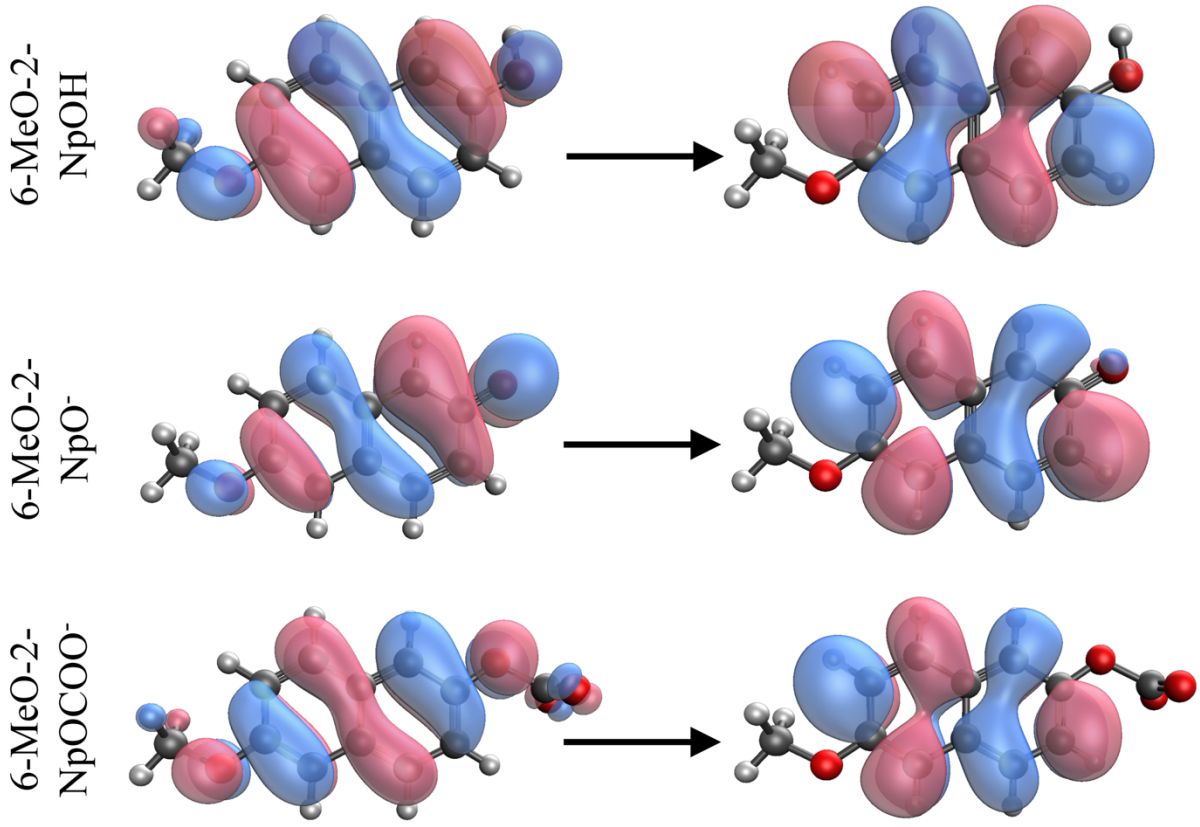

Figure S22: The natural transition orbitals (NTOs) for the $S_0 \rightarrow S_1$ transition of 6-MeO-2-NpOH, 6-MeO-2-NpO^-, and 6-MeO-2-$NpOCOO^-$. The NTOs were calculated at the ADC(2)/def2-tzvpd//ROKS-ωB97X-D/def2-SVPD level of theory at the excited state optimized geometry and plotted with an isovalue of 0.06.

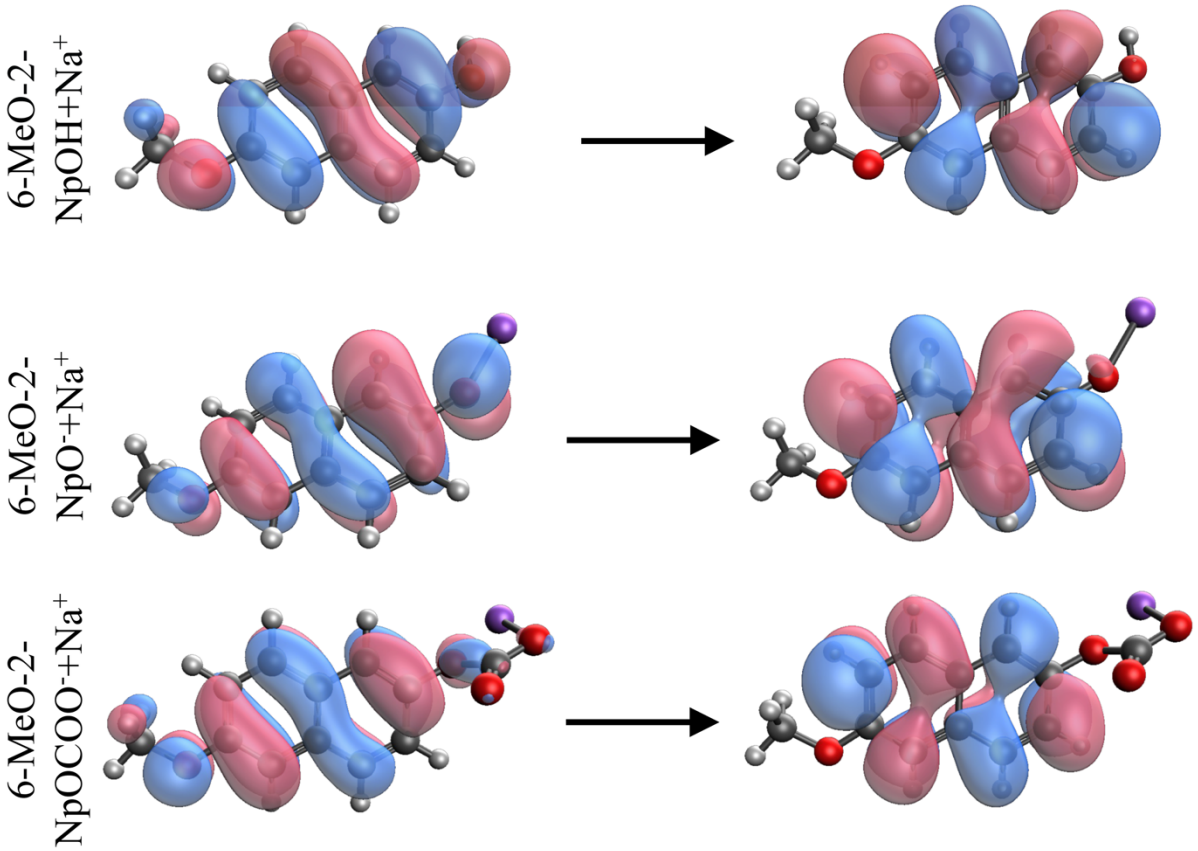

Figure S23: The natural transition orbitals (NTOs) for the $S_0 \rightarrow S_1$ transition of 6-MeO-2-NpOH, 6-MeO-2-$NpO^{-}+Na^{+}$, and 6-MeO-2-$NpOCOO^{-}+Na^{+}$. The NTOs were calculated at the ADC(2)/def2-tzvpd//ROKS-ωB97X-D/def2-SVPD level of theory at the ground state optimized geometry and plotted with an isovalue of 0.06.

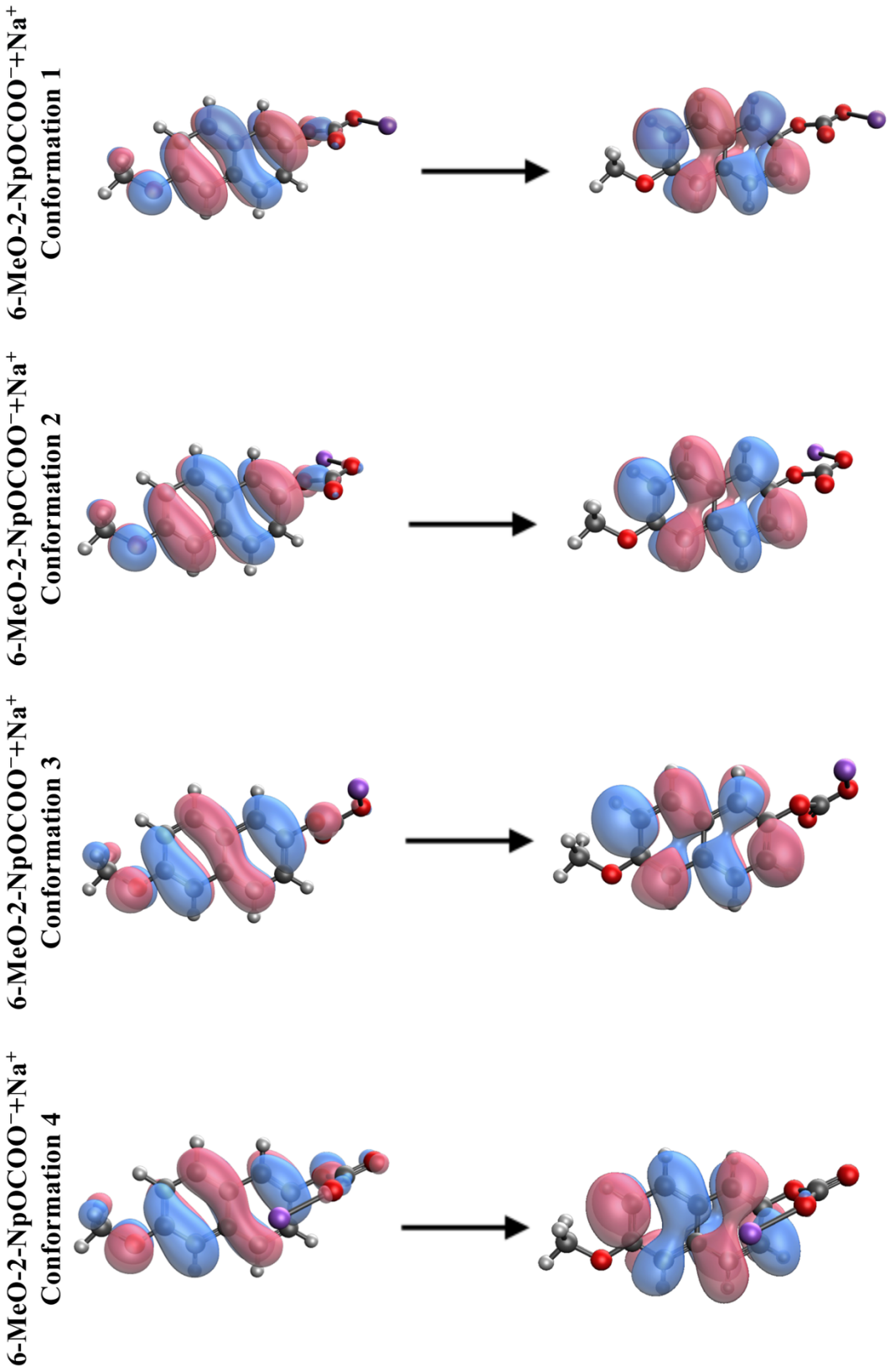

Figure S24: The natural transition orbitals (NTOs) for the $S_0 \rightarrow S_1$ transition of the different conformations of 6-MeO-2-NpOCOO$^-$+Na$^+$. The NTOs were calculated at the ADC(2)/def2-tzvpd//ROKS-ωB97X-D/def2-SVPD level of theory at the excited state optimized geometry and plotted with an isovalue of 0.06.

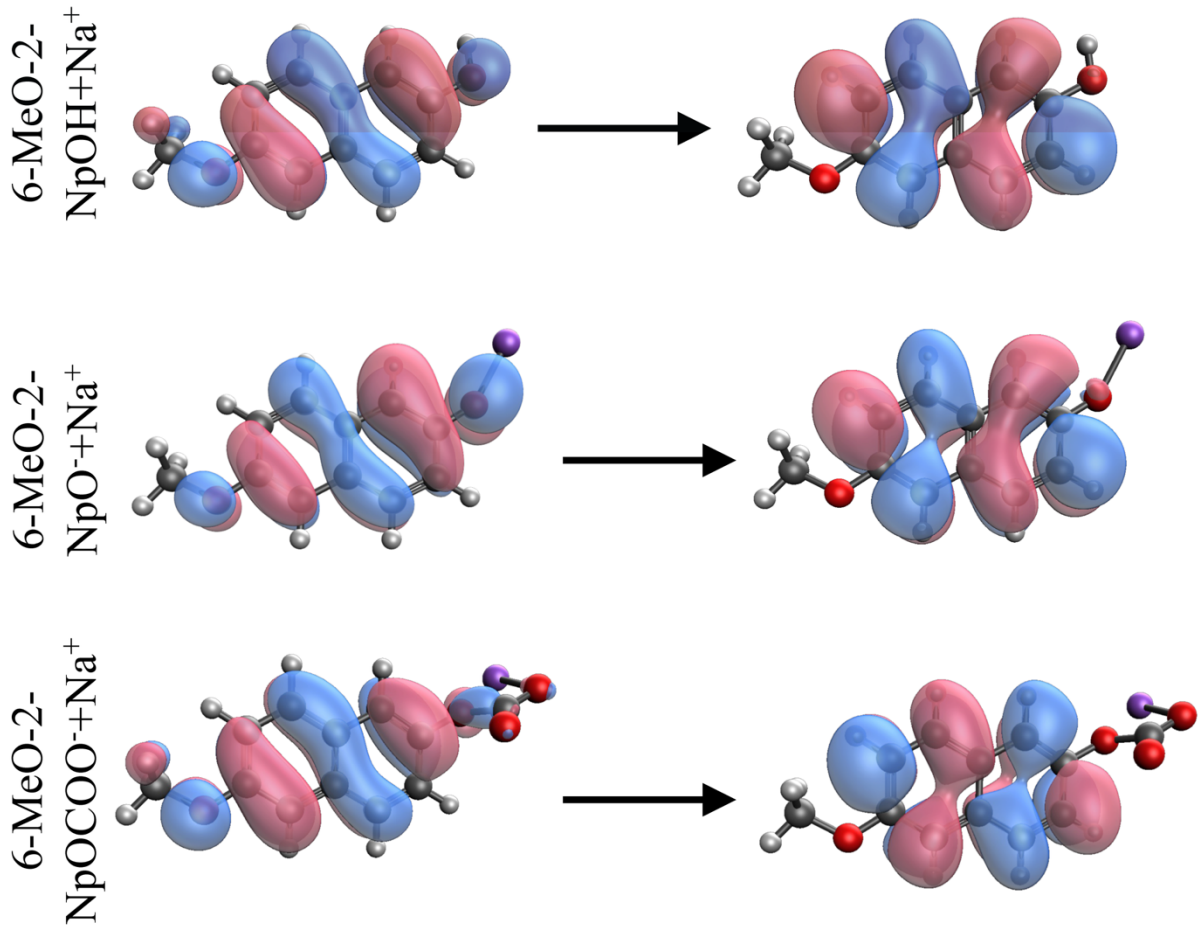

Figure S25: The natural transition orbitals (NTOs) for the $S_0 \rightarrow S_1$ transition of 6-MeO-2-NpOH, 6-MeO-2-NpO$^-$+Na$^+$, and 6-MeO-2-NpOCOO$^-$+Na$^+$. The NTOs were calculated at the ADC(2)/def2-tzvpd//ROKS-ωB97X-D/def2-SVPD level of theory at the excited state optimized geometry and plotted with an isovalue of 0.06.

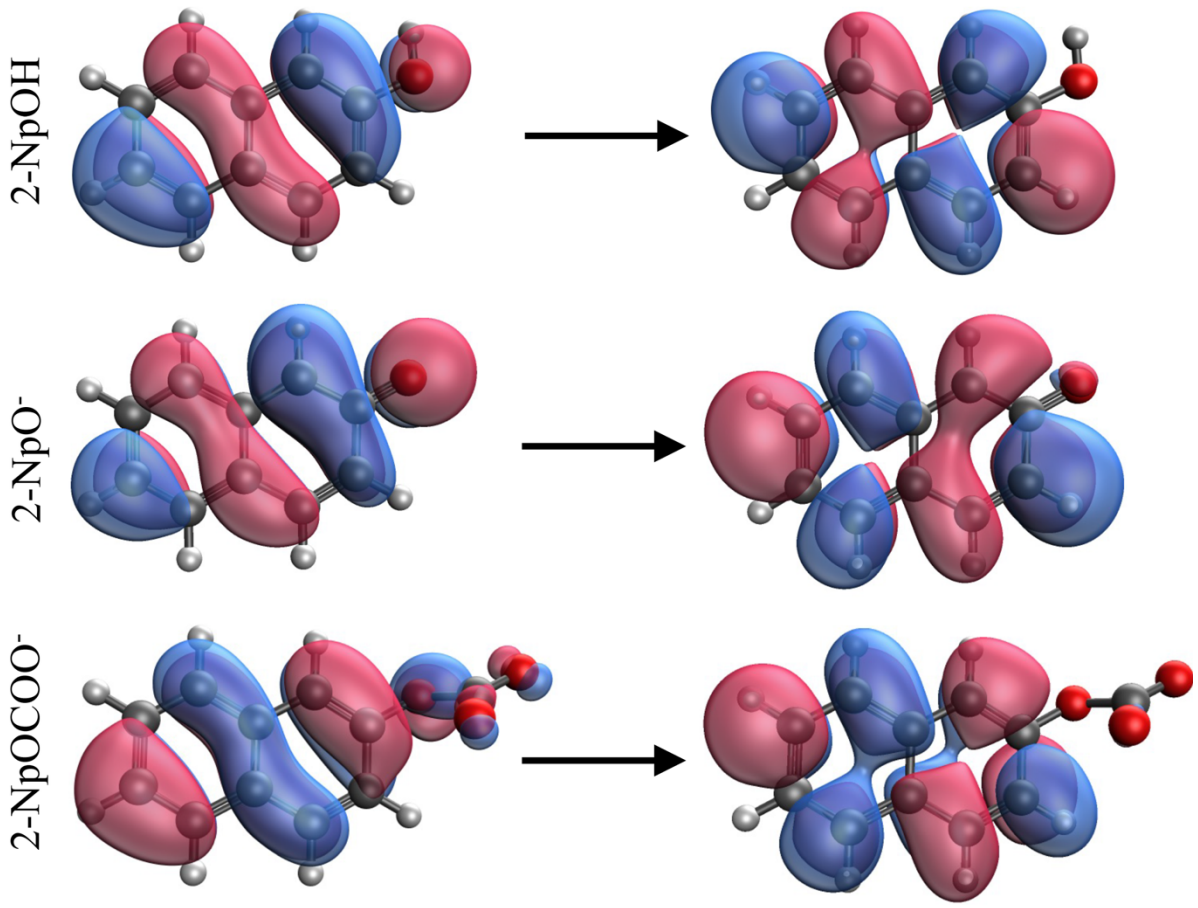

Figure S26: The natural transition orbitals (NTOs) for the $S_0 \rightarrow S_1$ transition of 2-NpOH, 2-NpO^-, and 2-$NpOCOO^-$. The NTOs were calculated at the ADC(2)/def2-tzvpd//ωB97X-D/def2-SVPD level of theory at the ground state optimized geometry and plotted with an isovalue of 0.06.

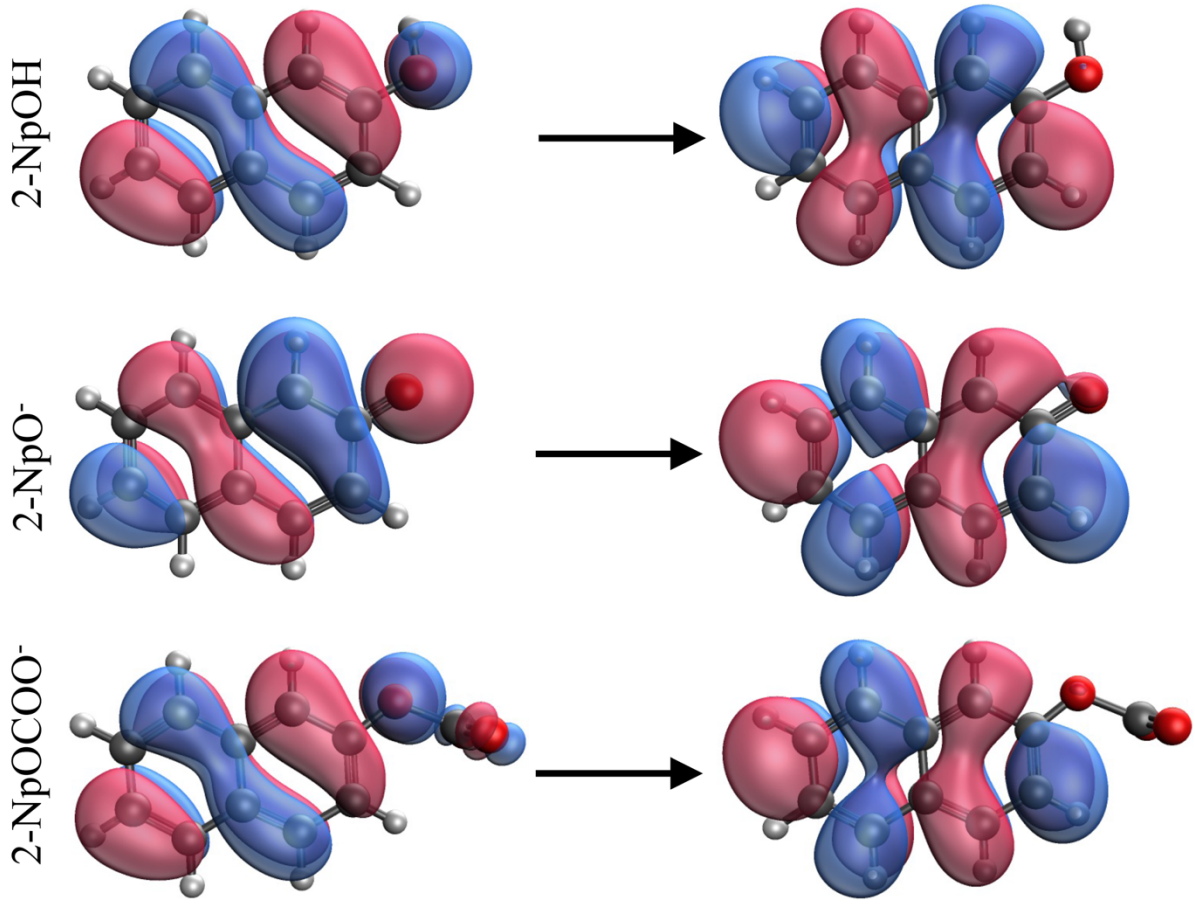

Figure S27: The natural transition orbitals (NTOs) for the $S_0 \rightarrow S_1$ transition of 2-NpOH, 2-NpO^-, and 2-$NpOCOO^-$. The NTOs were calculated at the ADC(2)/def2-tzvpd// ROKS-ωB97X-D/def2-SVPD level of theory at the excited state optimized geometry and plotted with an isovalue of 0.06.

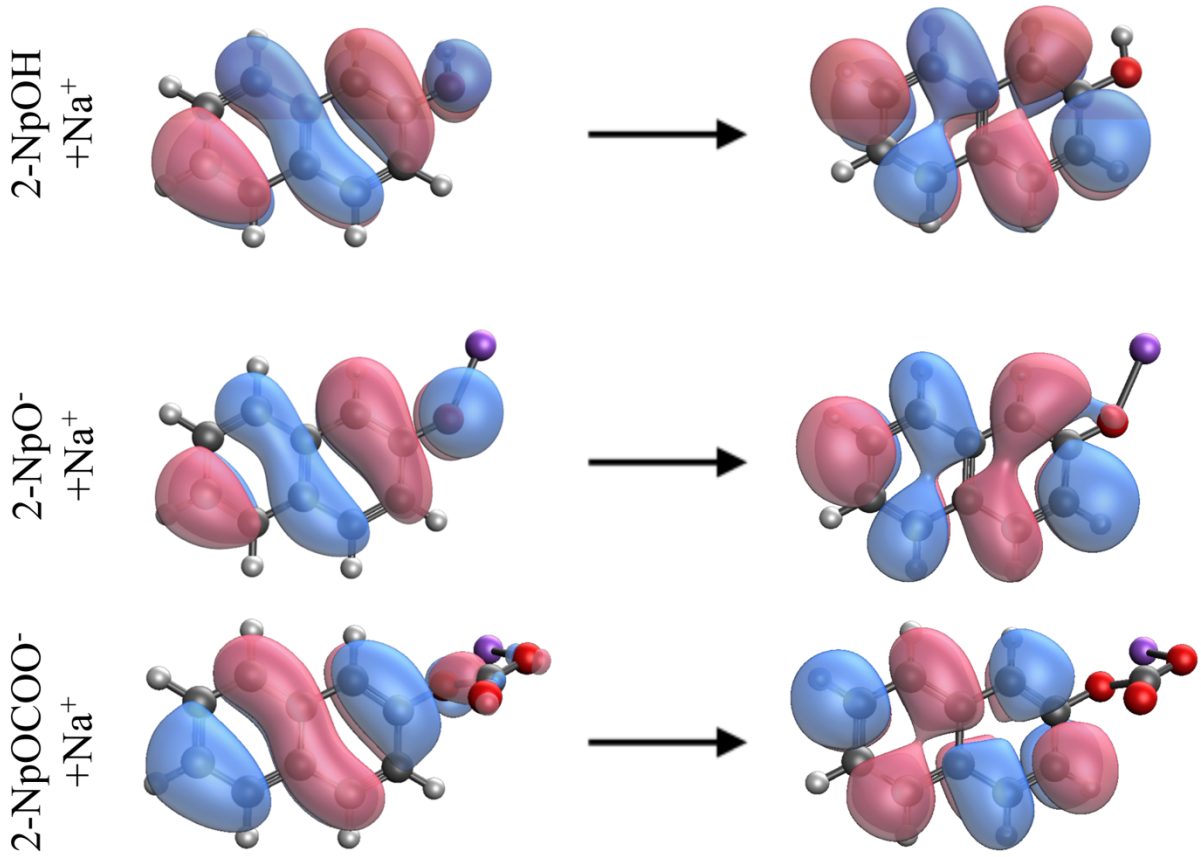

Figure S28: The natural transition orbitals (NTOs) for the $S_0 \rightarrow S_1$ transition of 2-NpOH, 2-NpO^-+Na^+, and 2-$NpOCOO^-$+Na^+. The NTOs were calculated at the ADC(2)/def2-tzvpd//ROKS-ωB97X-D/def2-SVPD level of theory at the ground state optimized geometry and plotted with an isovalue of 0.06.

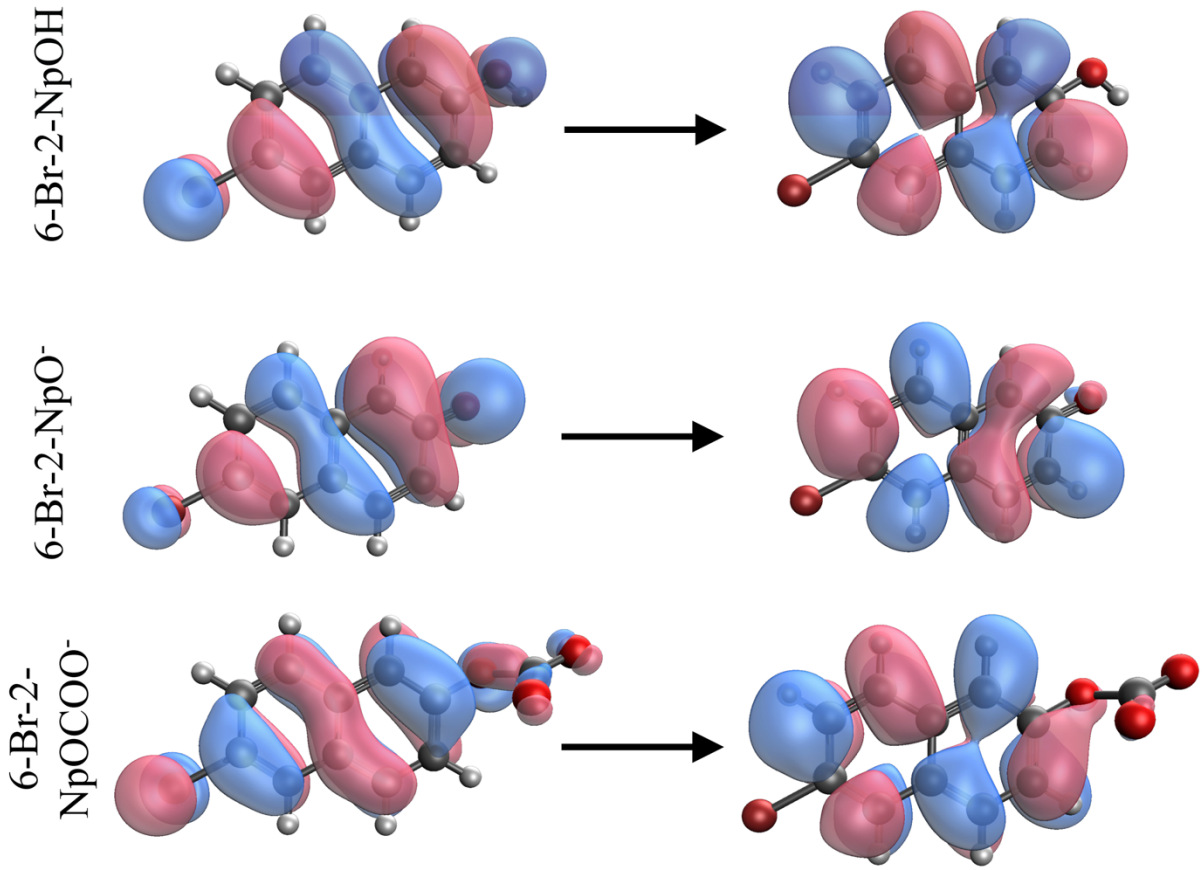

Figure S29: The natural transition orbitals (NTOs) for the $S_0 \rightarrow S_1$ transition of 6-Br-2-NpOH, 6-Br-2-NpO^-, and 6-Br-2-$NpOCOO^-$. The NTOs were calculated at the ADC(2)/def2-tzvpd//ωB97X-D/def2-SVPD level of theory at the ground state optimized geometry and plotted with an isovalue of 0.06.

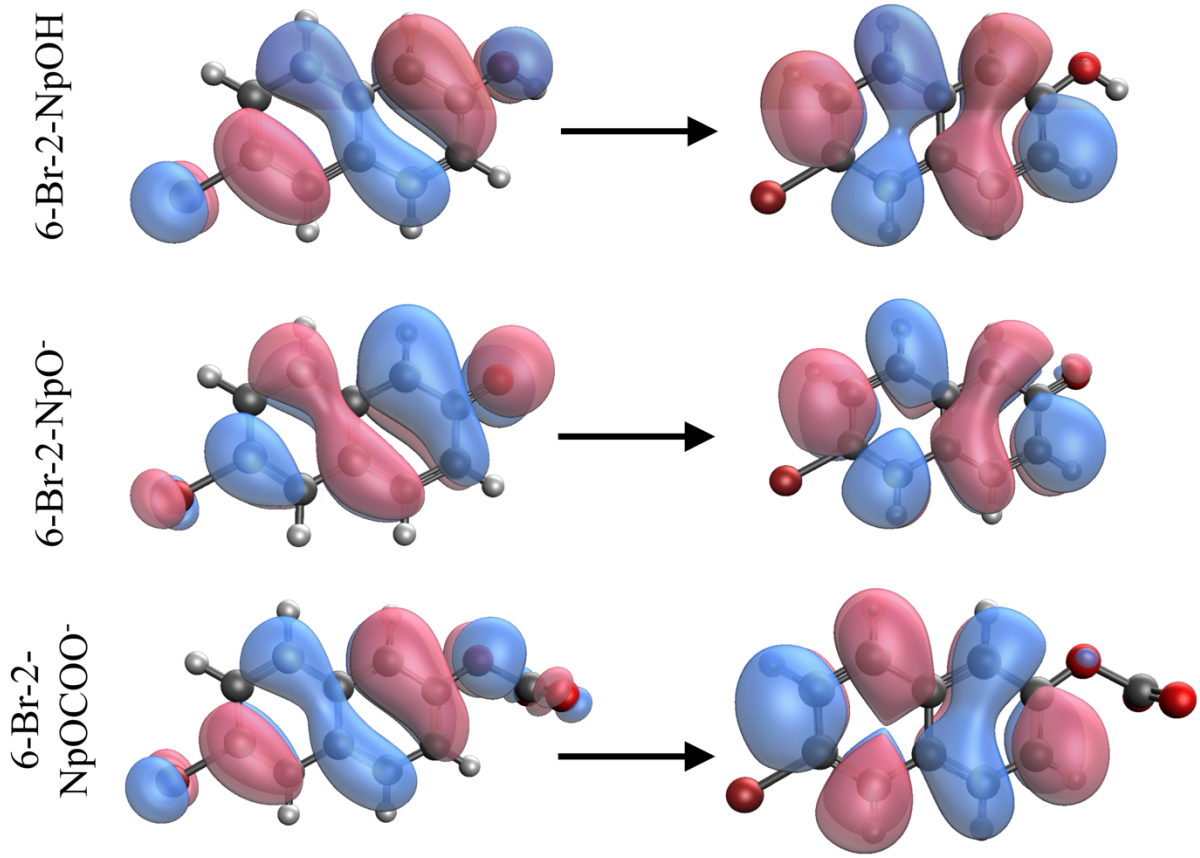

Figure S30: The natural transition orbitals (NTOs) for the $S_0 \rightarrow S_1$ transition of 6-Br-2-NpOH, 6-Br-2-NpO^-, and 6-Br-2-$NpOCOO^-$. The NTOs were calculated at the ADC(2)/def2-tzvpd//ROKS-ωB97X-D/def2-SVPD level of theory at the excited state optimized geometry and plotted with an isovalue of 0.06.

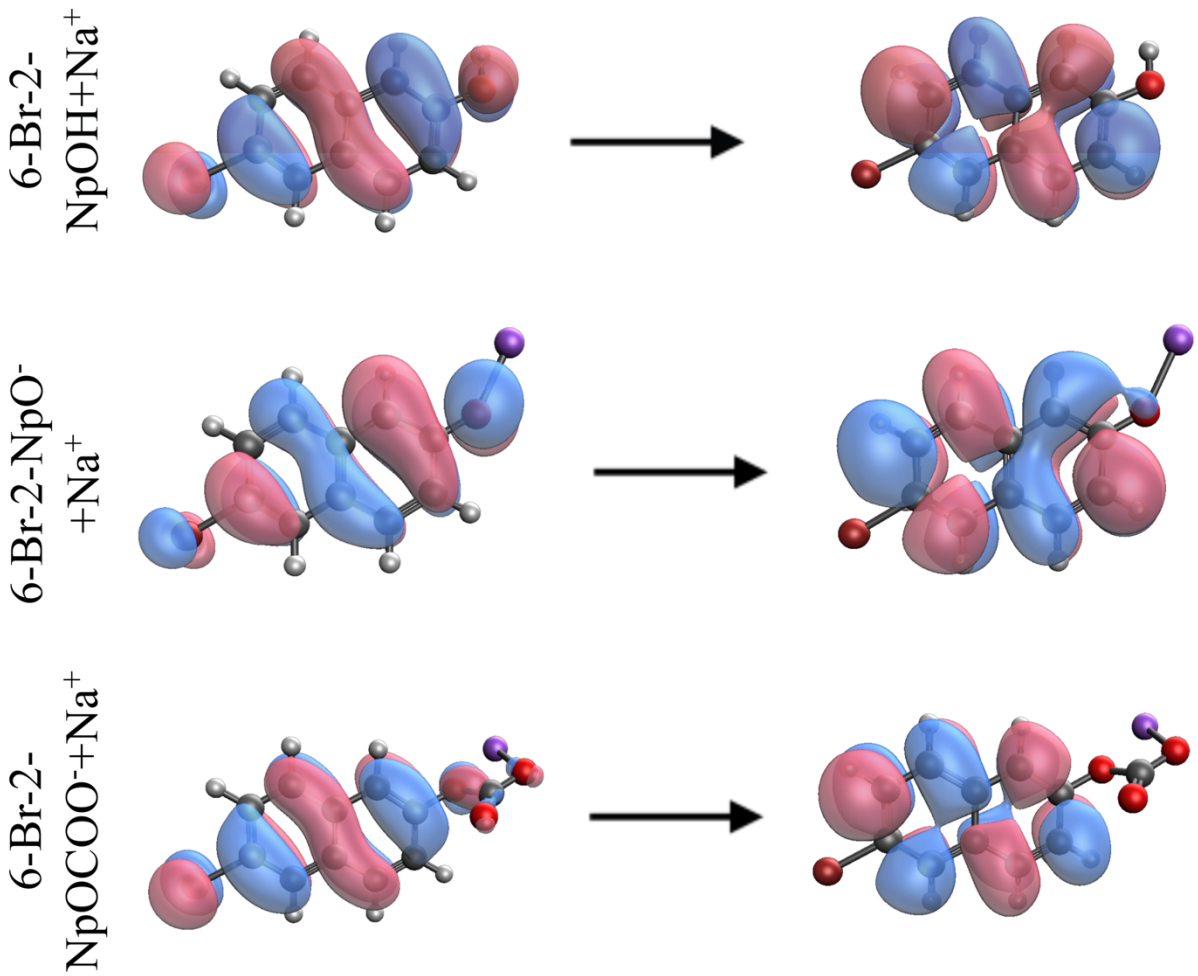

Figure S31: The natural transition orbitals (NTOs) for the $S_0 \rightarrow S_1$ transition of 6-Br-2-NpOH, 6-Br-2-NpO^-+Na^+, and 6-Br-2-$NpOCOO^-$+Na^+. The NTOs were calculated at the ADC(2)/def2-tzvpd//ROKS-ωB97X-D/def2-SVPD level of theory at the ground state optimized geometry and plotted with an isovalue of 0.06.

Förster Cycle Analysis

Table S17: Calculated ΔΔG for proton or CO_2 release with and without a contact ion pair with Na^+ for 6-MeO-2NpOH and 6-MeO-2pOCOO⁻.

	Zero-Point Corrected ΔΔG (eV)[a,b,c,d]	**Zero-Point Corrected $\Delta pK_a/\Delta pK_{CO_2}$[e]**
6-MeO-2-NpOH → 6-MeO-2-NpO⁻	-0.89	-15.02
6-MeO-2-NpOH → 6-MeO-2-NpO⁻+Na⁺	-0.55	-9.33
6-MeO-2-NpOCOO⁻ → 6-MeO-2-NpO⁻	-0.81	-13.68
6-MeO-2-NpOCOO⁻+Na⁺ Conf 1 → 6-MeO-2-NpO⁻+Na⁺	-0.73	-12.36
6-MeO-2-NpOCOO⁻+Na⁺ Conf 2 → 6-MeO-2-NpO⁻+Na⁺	-0.71	-11.93
6-MeO-2-NpOCOO⁻+Na⁺ Conf 3 → 6-MeO-2-NpO⁻+Na⁺	-0.70	-11.84
6-MeO-2-NpOCOO⁻+Na⁺ Conf 4 → 6-MeO-2-NpO⁻+Na⁺	-0.62	-10.40

[a]Calculations performed at the ADC(2)/def2-TZVPD//ωB97X-D/def2-SVPD level of theory with a PCM parameterized for THF. The resolution of identity approximation was used to accelerate the ADC(2) calculations.
[b]Excited state geometry optimizations performed using ROKS-ωB97X-D/def2-SVPD.
[c]$\Delta\Delta G = E_{00}^{Acid} - E_{00}^{Base}$, where E_{00}^{Base} is the adiabatic energy gap for 6-methoxy-2-naphtholate and E_{00}^{Acid} is the adiabatic energy gap of either 6-methoxy-2-naphthol (Brønsted photoacidity) or 6-methoxy-2-napthylcarbonate (Lewis photoacidity).
[d]For 6-MeO-2-NpOH and 6-MeO-2-NpO⁻+Na⁺, the ΔΔG was calculated using a thermal average of the 2 conformers with Boltzmann weights evaluated at room temperature. This analysis was performed at the ωB97M-V/def2-QZVPD//ωB97X-D/def2-SVPD level of theory.
[e]Calculated using $\Delta pK_a = \frac{\Delta\Delta G}{2.303RT}$, with T=298.15 K.

Figure S26 summarizes our calculated increase in thermodynamic driving force for proton/CO_2 release in the excited state relative to the ground state. Focusing first on the Bronsted photoacidity of 6-MeO-2-NpOH, we see that our calculations overestimate the magnitude of ΔΔG and hence ΔpK_a relative to the experimental values of ΔΔG=-0.37 eV and $\Delta pK_a = -6.29$. Importantly, including the effects of a contact ion pair between 6-MeO-2-NpO⁻ and Na^+ significantly improves agreement with experiment. Turning to 6-MeO-2-NpOCOO⁻, our calculations demonstrate Lewis photoacidity. As with 6-MeO-2-NpOH, our calculations overestimate the magnitude of ΔΔG and hence ΔpK_{CO_2}. As above, the agreement with experiment is improved by the addition of a Na^+ ion. We do note that the agreement with experiment is less good for 6-MeO-2-NpOCOO⁻+Na^+ than 6-MeO-2-NpOH.

Table S18: Calculated ΔΔG for proton or CO_2 release with and without a contact ion pair with Na^+ for 2-NpOH and 2-NpOCOO$^-$.

	Zero-Point Corrected ΔΔG (eV)[a,b,c,d]	**Zero-Point Corrected $\Delta pK_a/\Delta pK_{CO_2}$[e]**
2-NpOH → 2-NpO$^-$	-1.10	-18.64
2-NpOH → 2-NpO$^-$+Na$^+$	-0.72	-12.22
2-NpOCOO$^-$ → 2-NpO$^-$	-0.85	-14.41
2-NpOCOO$^-$+Na$^+$ Conf 1 → 2-NpO$^-$+Na$^+$	-0.91	-15.39
2-NpOCOO$^-$+Na$^+$ Conf 2 → 2-NpO$^-$+Na$^+$	-0.92	-15.52
2-NpOCOO$^-$+Na$^+$ Conf 3 → 2-NpO$^-$+Na$^+$	-0.92	-15.56
2-NpOCOO$^-$+Na$^+$ Conf 4 → 2-NpO$^-$+Na$^+$	-0.94	-15.85

[a]Calculations performed at the ADC(2)/def2-TZVPD//ωB97X-D/def2-SVPD level of theory with a PCM parameterized for THF. The resolution of identity approximation was used to accelerate the ADC(2) calculations.

[b]Excited state geometry optimizations performed using ROKS-ωB97X-D/def2-SVPD.

[c]$\Delta\Delta G = E_{00}^{Acid} - E_{00}^{Base}$, where E_{00}^{Base} is the adiabatic energy gap for 6-methoxy-2-naphtholate and E_{00}^{Acid} is the adiabatic energy gap of either 6-methoxy-2-naphthol (Brønsted photoacidity) or 6-methoxy-2-napthylcarbonate (Lewis photoacidity).

[d]For 6-MeO-2-NpOH and 6-MeO-2-NpO$^-$+Na$^+$, the ΔΔG was calculated using a thermal average of the 2 conformers with Boltzmann weights evaluated at room temperature. This analysis was performed at the ωB97M-V/def2-QZVPD//ωB97X-D/def2-SVPD level of theory.

[e]Calculated using $\Delta pK_a = \frac{\Delta\Delta G}{2.303RT}$, with T=298.15 K.

Table S19: Calculated ΔΔG for proton or CO_2 release with and without a contact ion pair with Na^+ for 6-Br-2NpOH and 6-Br-2NpOCOO$^-$.

	Zero-Point Corrected ΔΔG (eV)[a,b,c,d]	**Zero-Point Corrected $\Delta pK_a/\Delta pK_{CO_2}$[e]**
6-Br-2-NpOH → 6-Br-2-NpO$^-$	-1.10	-18.60
6-Br-2-NpOH → 6-Br-2-NpO$^-$+Na$^+$	-0.74	-12.57
6-Br-2-NpOCOO$^-$ → 6-Br-2-NpO$^-$	-0.83	-13.95
6-Br-2-NpOCOO$^-$+Na$^+$ Conf 1 → 6-Br-2-NpO$^-$+Na$^+$		
6-Br-2-NpOCOO$^-$+Na$^+$ Conf 2 → 6-Br-2-NpO$^-$+Na$^+$	-0.89	-15.08
6-Br-2-NpOCOO$^-$+Na$^+$ Conf 3 → 6-Br-2-NpO$^-$+Na$^+$	-0.90	-15.14
6-Br-2-NpOCOO$^-$+Na$^+$ Conf 4 → 6-Br-2-NpO$^-$+Na$^+$		

[a]Calculations performed at the ADC(2)/def2-TZVPD//ωB97X-D/def2-SVPD level of theory with a PCM parameterized for THF. The resolution of identity approximation was used to accelerate the ADC(2) calculations.

[b]Excited state geometry optimizations performed using ROKS-ωB97X-D/def2-SVPD.

[c]$\Delta\Delta G = E_{00}^{Acid} - E_{00}^{Base}$, where E_{00}^{Base} is the adiabatic energy gap for 6-methoxy-2-naphtholate and E_{00}^{Acid} is the adiabatic energy gap of either 6-methoxy-2-naphthol (Brønsted photoacidity) or 6-methoxy-2-napthylcarbonate (Lewis photoacidity).

[d]For 6-MeO-2-NpOH and 6-MeO-2-NpO$^-$+Na$^+$, the ΔΔG was calculated using a thermal average of the 2 conformers with Boltzmann weights evaluated at room temperature. This analysis was performed at the ωB97M-V/def2-QZVPD//ωB97X-D/def2-SVPD level of theory.

[e]Calculated using $\Delta pK_a = \frac{\Delta\Delta G}{2.303RT}$, with T=298.15 K.

Analysis of Photoacidity Descriptors

Table S20: Analysis of the change in charge at the oxygen atom responsible for photoacidity caused by electronic excitation for the 2-naphthols and the 2-naphthylcarbonates.[a]

	Δq^* (e)
6-methoxy-2-naphthol[b]	0.05
6-methoxy-2-naphthylcarbonate	0.10
2-naphthol[b]	0.07
2-naphthylcarbonate	0.13
6-bromo-2-naphthol[b]	0.07
6-bromo-2-naphthylcarbonate	0.13

[a]The change in the partial charge at oxygen atom of the alcohol group caused by electronic excitation. The calculation was performed at the excited state optimized geometry using Löwdin population analysis using the transition density matrix at the ADC(2)/def2-TZVPD level of theory.
[b]Thermal average of the 2 conformers with Boltzmann weights evaluated at room temperature at the ωB97M-V/def2-QZVPD//ωB97X-D/def2-SVPD level of theory.

Table S21: Analysis of the change in charge at the oxygen atom responsible for photoacidity caused by electronic excitation for the different conformers of the contact ion pair between the 2-naphthylcarbonates and Na^+.[a]

	Δq^* (e)[a]
6-methoxy-2-naphthylcarbonate + Na^+	
Conformer 1	0.03
Conformer 2	0.02
Conformer 3	0.02
Conformer 4	0.02
2-naphthylcarbonate + Na^+	
Conformer 1	0.06
Conformer 2	0.05
Conformer 3	0.04
Conformer 4	0.03
6-bromo-2-naphthylcarbonate + Na^+	
Conformer 1	
Conformer 2	0.05
Conformer 3	0.05
Conformer 4	

[a]The change in the partial charge at oxygen atom of the alcohol group caused by electronic excitation. The calculation was performed at the excited state optimized geometry using Löwdin population analysis using the transition density matrix at the ADC(2)/def2-TZVPD level of theory.

The analysis shown in Tables SP16-SP17 demonstrates that the $S_0 \rightarrow S_1$ electronic excitation causes a general shift of electron density away from the oxygen atom bound to the photoacidic proton or CO_2. This weakens the O-H or O-C bond, consistent with an increased thermodynamic driving force for the release of a proton or CO_2.

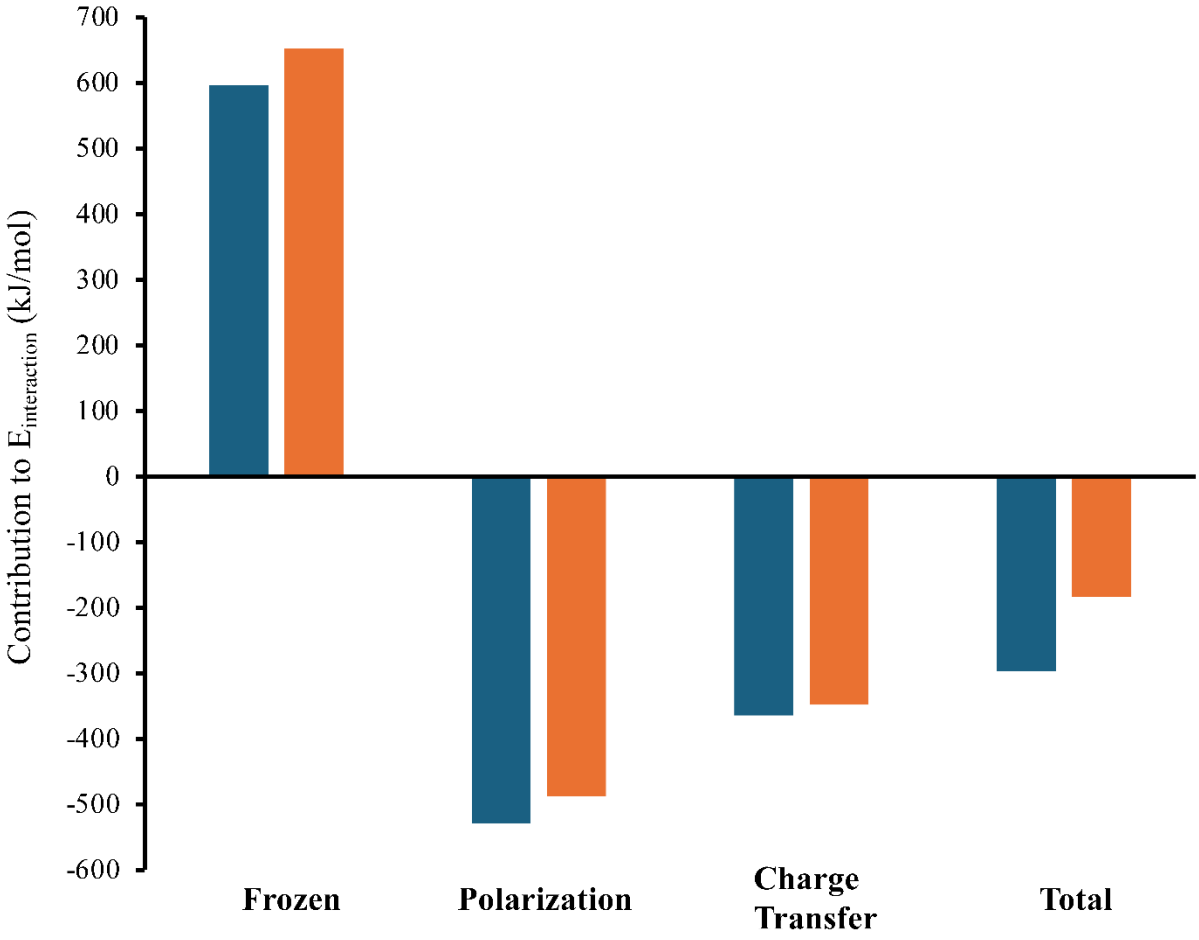

Figure S32: The results of energy decomposition analysis (EDA) of the dative bond in 6-MeO-2-NpOCOO$^-$+Na$^+$ performed at the ground state (blue) and excited state (orange) optimized geometry. The EDA analysis was performed using the second-generation absolutely localized molecular orbitals (ALMO-EDA II) methodology at the ωB97X-D/def2-TZVPPD level of theory. We used the state-specific maximum overlap method (MOM) to perform the EDA analysis on a non-Aufbau excited electron configuration. We performed the analysis at conformer 2 from Figure S16 and defined the molecular fragments as CO_2 and 6-Me-2-NpO$^-$+Na$^+$.

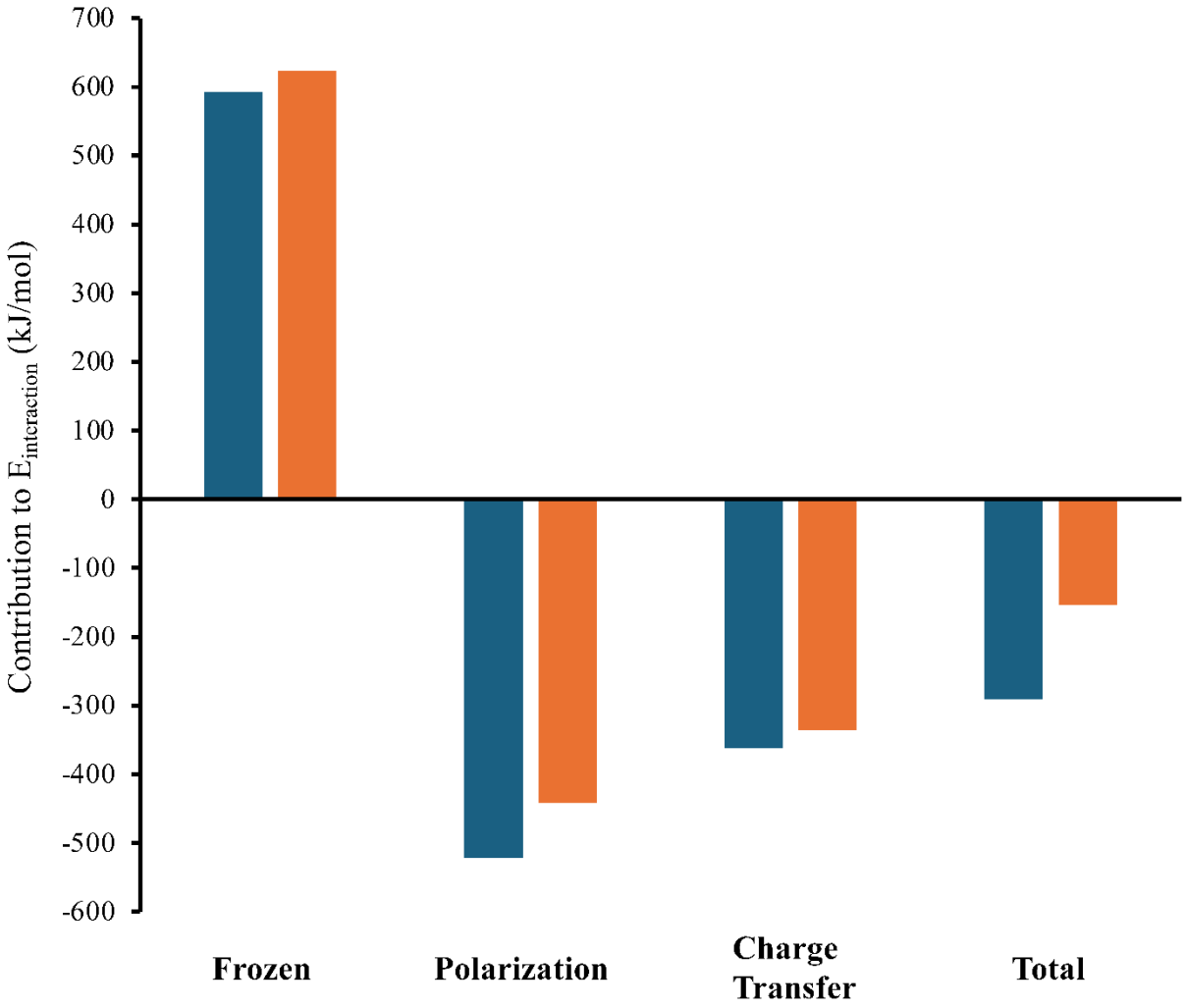

Figure S33: The results of energy decomposition analysis (EDA) of the dative bond in 2-NpOCOO^{-}+Na^{+} performed at the ground state (blue) and excited state (orange) optimized geometry. The EDA analysis was performed using the second-generation absolutely localized molecular orbitals (ALMO-EDA II) methodology at the ωB97X-D/def2-TZVPPD level of theory. We used the state-specific maximum overlap method (MOM) to perform the EDA analysis on a non-Aufbau excited electron configuration. We performed the analysis at conformer 2 from Figure S16 and defined the molecular fragments as CO_2 and 2-NpO^{-}+Na^{+}.

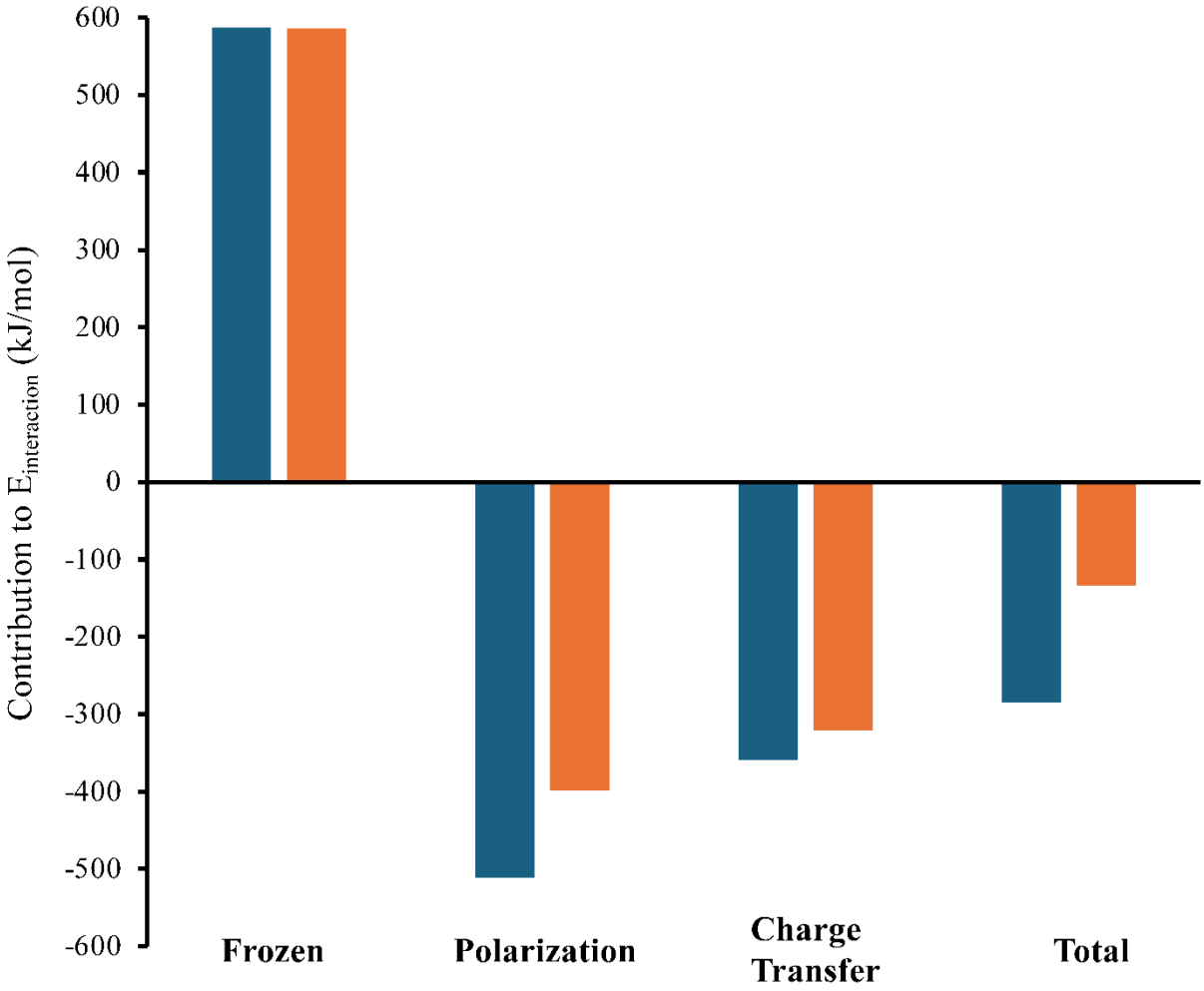

Figure S34: The results of energy decomposition analysis (EDA) of the dative bond in 6-Br-2-NpOCOO^{-}+Na^{+} performed at the ground state (blue) and excited state (orange) optimized geometry. The EDA analysis was performed using the second-generation absolutely localized molecular orbitals (ALMO-EDA II) methodology at the ωB97X-D/def2-TZVPPD level of theory. We used the state-specific maximum overlap method (MOM) to perform the EDA analysis on a non-Aufbau excited electron configuration. We performed the analysis at conformer 2 from Figure S16 and defined the molecular fragments as CO_2 and 6-Br-2-NpO^{-}+Na^{+}.

Table S22: Analysis of the different components of the interaction energy between 6-Meo-2-NpO^{-}+Na^{+} and CO_2 for 6-Meo-2-$NpOCOO^{-}$+Na^{+}.[a]

	$E_{interaction}$ at S_0 Geometry (kJ/mol)	$E_{interaction}$ at S_1 Geometry (kJ/mol)
Classical Electrostatics	-797.95	-641.28
Pauli Repulsion	1450.56	1349.07
Dispersion	-56.69	-55.50
Frozen	595.92	652.29
Polarization	-529.09	-487.27
Charge-Transfer	-364.58	-348.62
Total	-297.75	-183.60

[a]The EDA analysis was performed using the second-generation absolutely localized molecular orbitals (ALMO-EDA II) methodology at the ωB97X-D/def2-TZVPPD level of theory. We used the state-specific maximum overlap method (MOM) to perform the EDA analysis on a non-Aufbau excited electron configuration. The analysis was performed at conformer 2 from Figure S16.

Table S23: Analysis of the different components of the interaction energy between 2-NpO^{-}+Na^{+} and CO_2 for 2-$NpOCOO^{-}$+Na^{+}.[a]

	$E_{interaction}$ at S_0 Geometry (kJ/mol)	$E_{interaction}$ at S_1 Geometry (kJ/mol)
Classical Electrostatics	-788.20	-621.65
Pauli Repulsion	1437.97	1300.97
Dispersion	-56.64	-56.04
Frozen	593.13	623.28
Polarization	-521.87	-441.65
Charge-Transfer	-362.40	-335.64
Total	-291.14	-154.01

[a]The EDA analysis was performed using the second-generation absolutely localized molecular orbitals (ALMO-EDA II) methodology at the ωB97X-D/def2-TZVPPD level of theory. We used the state-specific maximum overlap method (MOM) to perform the EDA analysis on a non-Aufbau excited electron configuration. The analysis was performed at conformer 2 from Figure S16.

Table S24: Analysis of the different components of the interaction energy between 6-Br-2-NpO^{-}+Na^{+} and CO_2 for 6-Br-2-$NpOCOO^{-}$+Na^{+}.[a]

	$E_{interaction}$ at S_0 Geometry (kJ/mol)	$E_{interaction}$ at S_1 Geometry (kJ/mol)
Classical Electrostatics	-778.28	-598.92
Pauli Repulsion	1421.76	1241.42
Dispersion	-56.64	-55.97
Frozen	586.84	586.53
Polarization	-511.40	-399.06
Charge-Transfer	-359.88	-321.29
Total	-284.45	-133.81

[a]The EDA analysis was performed using the second-generation absolutely localized molecular orbitals (ALMO-EDA II) methodology at the ωB97X-D/def2-TZVPPD level of theory. We used the state-specific maximum overlap method (MOM) to perform the EDA analysis on a non-Aufbau excited electron configuration. The analysis was performed at conformer 2 from Figure S16.

Analysis of Excited State CO_2 Release

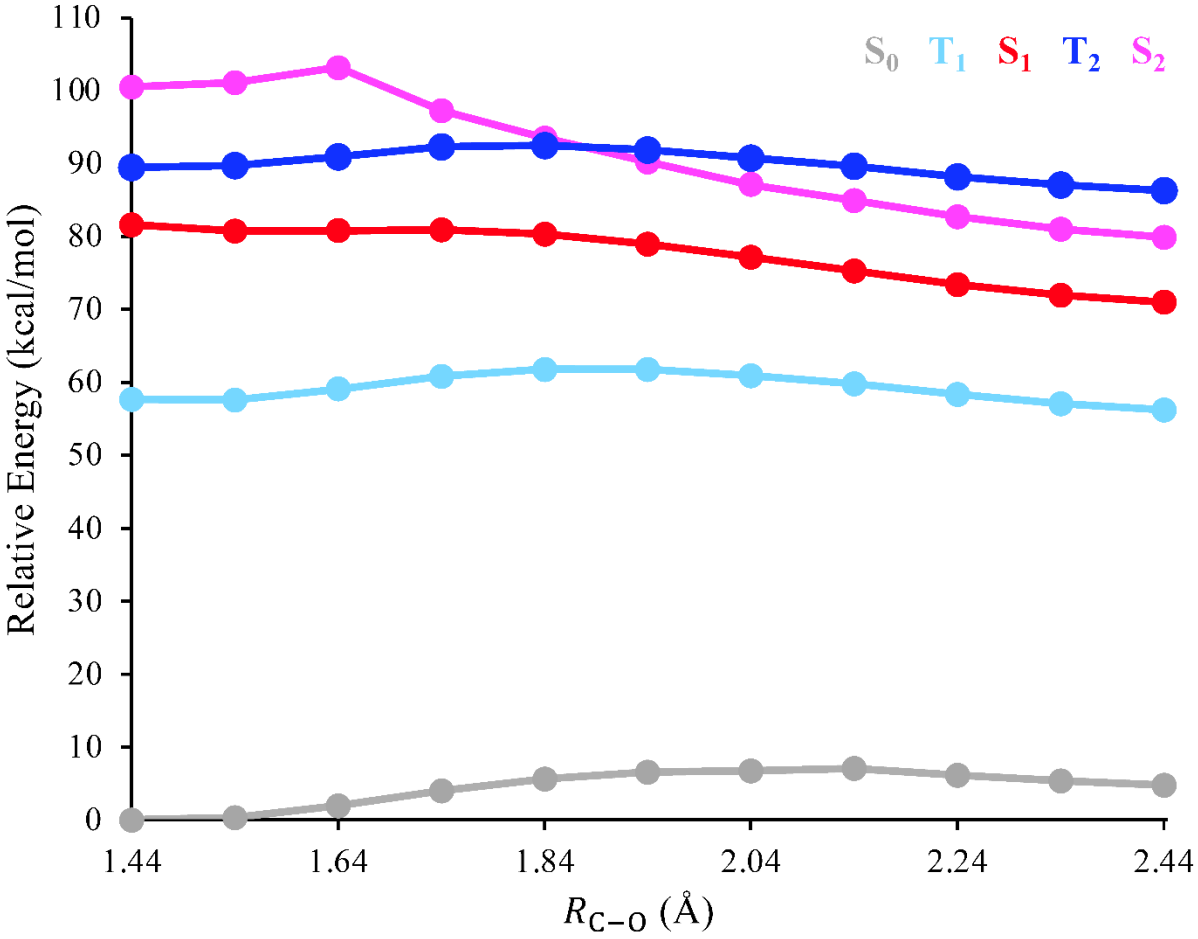

Figure S35: Potential energy curves associated with stretching the dative bond in 6-MeO-2-NpOCOO^{-}+Na^{+}, $R_{C\text{-}O}$, for the S_0- S_2 and T_1-T_2 states. The geometries were obtained from a relaxed scan performed at the ROKS-ωB97X-D/def2-SVPD level of theory, while the energies were evaluated using ADC(2)/def2-TZVPD. The S_1 state is shown to remain well-separated from other states throughout the scan.

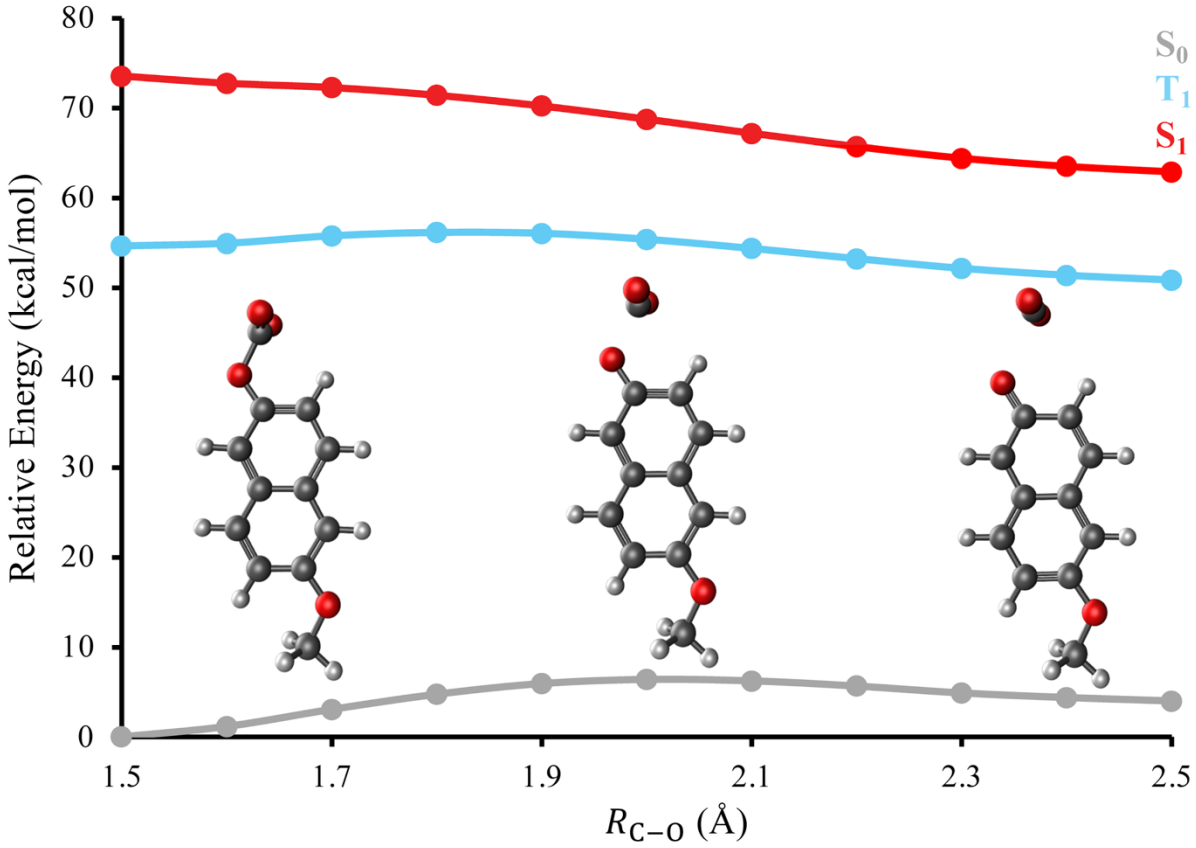

Figure S36: Potential energy curves associated with stretching the dative bond in 6-MeO-2-NpOCOO$^-$, $R_{C\text{-}O}$, for the S_0, S_1, and T_1 states. The geometries were obtained from a relaxed scan performed at the ROKS-ωB97X-D/def2-SVPD level of theory, while the energies were evaluated using ADC(2)/def2-TZVPD. In the absence of forming a contact ion pair with Na^+, we were unable to identify a transition state barrier for CO_2 release on S_1.

References:

(1) Delibas, B.; Cotton, D.; Sudhakaran, K. P.; Dawlaty, J. M. Evaluation of Aliphatic Alcohols for CO_2 Capture Using the Characteristic Carbonate Frequency. *ChemSusChem* **2025**, *18* (8), e202402288. https://doi.org/10.1002/cssc.202402288.

(2) Chai, J.-D.; Head-Gordon, M. Long-Range Corrected Hybrid Density Functionals with Damped Atom–Atom Dispersion Corrections. *Phys. Chem. Chem. Phys.* **2008**, *10* (44), 6615. https://doi.org/10.1039/b810189b.

(3) Chai, J.-D.; Head-Gordon, M. Systematic Optimization of Long-Range Corrected Hybrid Density Functionals. *J. Chem. Phys.* **2008**, *128* (8), 084106. https://doi.org/10.1063/1.2834918.

(4) Filatov, M.; Shaik, S. A Spin-Restricted Ensemble-Referenced Kohn–Sham Method and Its Application to Diradicaloid Situations. *Chem. Phys. Lett.* **1999**, *304* (5–6), 429–437. https://doi.org/10.1016/S0009-2614(99)00336-X.

(5) Hait, D.; Zhu, T.; McMahon, D. P.; Van Voorhis, T. Prediction of Excited-State Energies and Singlet–Triplet Gaps of Charge-Transfer States Using a Restricted Open-Shell Kohn–Sham Approach. *J. Chem. Theory Comput.* **2016**, *12* (7), 3353–3359. https://doi.org/10.1021/acs.jctc.6b00426.

(6) Kowalczyk, T.; Tsuchimochi, T.; Chen, P.-T.; Top, L.; Van Voorhis, T. Excitation Energies and Stokes Shifts from a Restricted Open-Shell Kohn-Sham Approach. *J. Chem. Phys.* **2013**, *138* (16), 164101. https://doi.org/10.1063/1.4801790.

(7) Epifanovsky, E.; Gilbert, A. T. B.; Feng, X.; Lee, J.; Mao, Y.; Mardirossian, N.; Pokhilko, P.; White, A. F.; Coons, M. P.; Dempwolff, A. L.; Gan, Z.; Hait, D.; Horn, P. R.; Jacobson, L. D.; Kaliman, I.; Kussmann, J.; Lange, A. W.; Lao, K. U.; Levine, D. S.; Liu, J.; McKenzie, S. C.; Morrison, A. F.; Nanda, K. D.; Plasser, F.; Rehn, D. R.; Vidal, M. L.; You, Z.-Q.; Zhu, Y.; Alam, B.; Albrecht, B. J.; Aldossary, A.; Alguire, E.; Andersen, J. H.; Athavale, V.; Barton, D.; Begam, K.; Behn, A.; Bellonzi, N.; Bernard, Y. A.; Berquist, E. J.; Burton, H. G. A.; Carreras, A.; Carter-Fenk, K.; Chakraborty, R.; Chien, A. D.; Closser, K. D.; Cofer-Shabica, V.; Dasgupta, S.; De Wergifosse, M.; Deng, J.; Diedenhofen, M.; Do, H.; Ehlert, S.; Fang, P.-T.; Fatehi, S.; Feng, Q.; Friedhoff, T.; Gayvert, J.; Ge, Q.; Gidofalvi, G.; Goldey, M.; Gomes, J.; González-Espinoza, C. E.; Gulania, S.; Gunina, A. O.; Hanson-Heine, M. W. D.; Harbach, P. H. P.; Hauser, A.; Herbst, M. F.; Hernández Vera, M.; Hodecker, M.; Holden, Z. C.; Houck, S.; Huang, X.; Hui, K.; Huynh, B. C.; Ivanov, M.; Jász, Á.; Ji, H.; Jiang, H.; Kaduk, B.; Kähler, S.; Khistyaev, K.; Kim, J.; Kis, G.; Klunzinger, P.; Koczor-Benda, Z.; Koh, J. H.; Kosenkov, D.; Koulias, L.; Kowalczyk, T.; Krauter, C. M.; Kue, K.; Kunitsa, A.; Kus, T.; Ladjánszki, I.; Landau, A.; Lawler, K. V.; Lefrancois, D.; Lehtola, S.; Li, R. R.; Li, Y.-P.; Liang, J.; Liebenthal, M.; Lin, H.-H.; Lin, Y.-S.; Liu, F.; Liu, K.-Y.; Loipersberger, M.; Luenser, A.; Manjanath, A.; Manohar, P.; Mansoor, E.; Manzer, S. F.; Mao, S.-P.; Marenich, A. V.; Markovich, T.; Mason, S.; Maurer, S. A.; McLaughlin, P. F.; Menger, M. F. S. J.; Mewes, J.-M.; Mewes, S. A.; Morgante, P.; Mullinax, J. W.; Oosterbaan, K. J.; Paran, G.; Paul, A. C.; Paul, S. K.; Pavošević, F.; Pei, Z.; Prager, S.; Proynov, E. I.; Rák, Á.; Ramos-Cordoba, E.; Rana, B.; Rask, A. E.; Rettig, A.; Richard, R. M.; Rob, F.; Rossomme, E.; Scheele, T.; Scheurer, M.; Schneider, M.; Sergueev, N.; Sharada, S. M.; Skomorowski, W.; Small, D. W.; Stein, C. J.; Su, Y.-C.; Sundstrom, E. J.; Tao, Z.; Thirman, J.; Tornai, G. J.; Tsuchimochi, T.; Tubman, N. M.; Veccham, S. P.; Vydrov, O.; Wenzel, J.; Witte, J.; Yamada, A.; Yao, K.; Yeganeh, S.; Yost, S. R.; Zech, A.; Zhang, I. Y.; Zhang, X.; Zhang, Y.; Zuev, D.; Aspuru-Guzik, A.; Bell, A. T.; Besley, N. A.; Bravaya, K. B.; Brooks, B. R.; Casanova, D.; Chai, J.-D.; Coriani, S.; Cramer, C. J.; Cserey, G.; DePrince, A. E.; DiStasio, R. A.; Dreuw, A.; Dunietz, B. D.; Furlani, T. R.; Goddard, W. A.; Hammes-Schiffer, S.; Head-Gordon, T.;

Hehre, W. J.; Hsu, C.-P.; Jagau, T.-C.; Jung, Y.; Klamt, A.; Kong, J.; Lambrecht, D. S.; Liang, W.; Mayhall, N. J.; McCurdy, C. W.; Neaton, J. B.; Ochsenfeld, C.; Parkhill, J. A.; Peverati, R.; Rassolov, V. A.; Shao, Y.; Slipchenko, L. V.; Stauch, T.; Steele, R. P.; Subotnik, J. E.; Thom, A. J. W.; Tkatchenko, A.; Truhlar, D. G.; Van Voorhis, T.; Wesolowski, T. A.; Whaley, K. B.; Woodcock, H. L.; Zimmerman, P. M.; Faraji, S.; Gill, P. M. W.; Head-Gordon, M.; Herbert, J. M.; Krylov, A. I. Software for the Frontiers of Quantum Chemistry: An Overview of Developments in the Q-Chem 5 Package. *J. Chem. Phys.* **2021**, *155* (8), 084801. https://doi.org/10.1063/5.0055522.

(8) Dempwolff, A. L.; Paul, A. C.; Belogolova, A. M.; Trofimov, A. B.; Dreuw, A. Intermediate State Representation Approach to Physical Properties of Molecular Electron-Detached States. I. Theory and Implementation. *J. Chem. Phys.* **2020**, *152* (2), 024113. https://doi.org/10.1063/1.5137792.

(9) Schirmer, J.; Trofimov, A. B. Intermediate State Representation Approach to Physical Properties of Electronically Excited Molecules. *J. Chem. Phys.* **2004**, *120* (24), 11449–11464. https://doi.org/10.1063/1.1752875.

(10) Mardirossian, N.; Head-Gordon, M. *ω* B97M-V: A Combinatorially Optimized, Range-Separated Hybrid, Meta-GGA Density Functional with VV10 Nonlocal Correlation. *J. Chem. Phys.* **2016**, *144* (21), 214110. https://doi.org/10.1063/1.4952647.

(11) Mao, Y.; Loipersberger, M.; Horn, P. R.; Das, A.; Demerdash, O.; Levine, D. S.; Prasad Veccham, S.; Head-Gordon, T.; Head-Gordon, M. From Intermolecular Interaction Energies and Observable Shifts to Component Contributions and Back Again: A Tale of Variational Energy Decomposition Analysis. *Annu. Rev. Phys. Chem.* **2021**, *72* (1), 641–666. https://doi.org/10.1146/annurev-physchem-090419-115149.

(12) Mao, Y.; Montoya-Castillo, A.; Markland, T. E. Excited State Diabatization on the Cheap Using DFT: Photoinduced Electron and Hole Transfer. *J. Chem. Phys.* **2020**, *153* (24), 244111. https://doi.org/10.1063/5.0035593.

(13) *6-Bromo-2-naphthol | 15231-91-1*. ChemicalBook. https://www.chemicalbook.com/ChemicalProductProperty_EN_CB8731186.htm (accessed 2025-08-08).

(14) *Oxidation of Hazardous Organics in a Two-Phase Fluorocarbon-Water System*. https://doi.org/10.1089/hwm.1986.3.405.

(15) *6-Methoxy-2-naphthol CAS#: 5111-66-0*. https://m.chemicalbook.com/ProductChemicalPropertiesCB4121707_EN.htm (accessed 2025-08-08).